IEEE Access
Multidisciplinary ⋮ Rapid Review ⋮ Open Access Journal

Received 11 December 2025, accepted 16 January 2026, date of publication 26 January 2026, date of current version 12 February 2026.

Digital Object Identifier 10.1109/ACCESS.2026.3657951

RESEARCH ARTICLE

Radio-Frequency Toroid Susceptometry of Magnetic Nanoparticles: What Goes Around Comes Around

RONALD B. GOLDFARB, (Life Fellow, IEEE)
National Institute of Standards and Technology, Boulder, CO 80305, USA

e-mail: r.goldfarb@ieee.org; ron.goldfarb@nist.gov

This work was supported by the CHIPS Metrology Program as part of CHIPS for America, National Institute of Standards and Technology (NIST), U.S. Department of Commerce, and the NIST Physical Measurement Laboratory.

ABSTRACT The intrinsic magnetic susceptibility of noninteracting magnetic nanoparticles is calculated from the measured complex radio-frequency susceptibility of dipolar-coupled particles in colloidal suspension. The susceptibility, derived from the impedance of toroidal specimens in a shorted coaxial transmission line, requires no adjustment for demagnetizing factors. Three established models for interacting superparamagnetic particles — the Weiss molecular-field model, the Onsager model, and the modified mean-field model — are extended to magnetically viscous particles at frequencies above their Néel relaxation frequency. Magnetic figures of merit for nanoparticles are the real and imaginary parts of complex intrinsic susceptibility scaled by particle concentration. The work seeks to promote standard characterization methods for interlaboratory comparison of realistic distributions of magnetic nanoparticles at radio frequencies.

INDEX TERMS Colloids, dipole interactions, ferrofluids, impedance analyzers, magnetic relaxation, magnetic susceptibility, magnetic viscosity, magnetostatic interactions, nanoparticles, permeability, permeameters, radio frequency, standards, superparamagnetism, susceptometers, toroids.

I. PROLOGUE

A. APPLICATIONS OF NANOPARTICLES

Many applications of magnetic nanoparticles and their colloidal suspensions are biomedical: contrast agents for magnetic resonance imaging, tracers for magnetic particle imaging, hysteretic heating elements for antitumor hyperthermia, carriers for targeted drug and gene delivery, molecular complexes for magnetic transfection of cells, functionalized particles for biomolecule and cell concentration and separation, and sensitive detection tags for lateral-flow immunoassays and biosensor arrays.

Other applications are electronic (high-frequency inductors and transformers for switching converters for on-chip power delivery, radio-frequency filters and phase shifters, microwave isolators and circulators, microwave absorbers, electrodes for supercapacitors); mechanical (dampers, vibration absorbers, seals, vacuum rotary feedthroughs); and physical (ferromagnetic domain visualization, management of heat transfer, magnetic recording media, magnetic separation of catalysts, printer inks).

In some applications of nanoscale iron oxide, the iron is more important than the particles' magnetic properties: catalytic degradation of microbes, fungi, and organic pollutants by the formation of reactive oxygen species via the Fenton reaction; adsorbents in water treatment; intravenous infusion of non-stoichiometric magnetite for iron-deficiency anemia; and ultraviolet radiation protection in paint pigments.

Radio-frequency magnetic characterization is directly relevant to many biomedical and electronic applications. For many applications and interlaboratory comparisons, it would be useful to know the intrinsic susceptibility of noninteracting magnetic nanoparticles. However, interparticle interactions always affect susceptibility measurements. In this article, the intrinsic magnetic susceptibility of noninteracting particles is derived from their measured complex susceptibility at radio frequencies and three established models for interacting superparamagnetic particles.

The associate editor coordinating the review of this manuscript and approving it for publication was Diana Leitao.

© 2026 The Authors. This work is licensed under a Creative Commons Attribution-NonCommercial-NoDerivatives 4.0 License.
For more information, see https://creativecommons.org/licenses/by-nc-nd/4.0/

The specimens used for measurement are representative of single-domain ferromagnetic nanoparticles, distributed in size, such as those used in actual engineering and biomedical applications. They do not satisfy the traditional criteria for superparamagnetism at ambient temperature [1]. They are below their blocking temperatures and their magnetization is hysteretic in magnetic field at radio frequencies. Nevertheless, these magnetically viscous[1] particles can still be analyzed using classic superparamagnetic theory: The modulus of the complex radio-frequency susceptibility masks the phase lag due to magnetic viscosity; quasi-static magnetization curves scale as a function of magnetic field divided by temperature.

B. SUPERPARAMAGNETISM

Magnetic nanoparticles are superparamagnetic above their blocking temperatures, which depend on the material, particle size, and measurement field and frequency. The magnetization of ensembles of particles is different from that of individual anisotropic particles, which actually exhibit discrete switching events as a function of time [3], [4], [5], [6]. Similarly, magnetic susceptibility (the initial slope of the magnetization–field curve) of a collection of particles averages the behavior of individual particles.

Magnetic nanoparticles are single-domain ferromagnets that behave as macrospins. In the absence of shape and magnetocrystalline anisotropy, their magnetic moments align in an applied magnetic field, subject to misalignment due to thermal activation. That is, superparamagnetic particles behave as paramagnetic polar atoms, ions, or molecules. Just as described by Bean and Livingston [2], an assembly of isotropic magnetic particles is analogous to atomic paramagnetism except for their large moments.[2]

As recounted by Bean and Jacobs [8], Montgomery [9] first hypothesized that the magnetization of single-domain ferromagnetic particles in colloidal suspension would follow a Langevin function. This was later verified by Elmore [10] and cited by Bean and Livingston [2] as an example of superparamagnetism.

C. DEMAGNETIZING FACTORS FOR SUPERPARAMAGNETIC COMPOSITES

Measured external susceptibilities of specimens must be corrected for demagnetizing factors to obtain the internal susceptibilities characteristic of materials. The demagnetizing factors for composites of superparamagnetic particles have special considerations.

1) DEMAGNETIZING FACTORS FOR PARAMAGNETS

A composite of *paramagnetic* particles has an effective demagnetizing factor that accounts for the demagnetizing factor of the particles (usually considered to be spherical) and that of the composite medium (for example, a disk). The intrinsic internal susceptibility of the composite can be obtained by correcting the measured external susceptibility by an effective demagnetizing factor N_{eff}, sometimes calculated using an interpolation formula [11], [12]:

$$N_{eff} = N_c\phi + N_p\,(1-\phi)\,, \tag{1}$$

where N_c is the demagnetizing factor of the composite, ϕ is the filling fraction, and N_p is the demagnetizing factor of a particle (equal to 1/3 for spheres).[3] The particles' demagnetizing field is $H_d = -N_{eff}M_p$, where the magnetization M_p is the magnetic moment m (attributable to all the particle moments) divided by the total volume of the particles V_p (equal to ϕ times the volume V of the composite). The internal field of the particles is[4]

$$\begin{aligned} H_{int,p} &= H_{ext} - N_{eff}M_p = H_{ext} - N_{eff}\frac{m}{V_p} \\ &= H_{ext} - N_{eff}\frac{m}{\phi V}. \end{aligned} \tag{2}$$

The internal susceptibility of the particles is

$$\begin{aligned} \chi_{int,p} &= \frac{M_p}{H_{int,p}} = \frac{M_p}{H_{ext} - N_{eff}M_p} = \frac{\chi_{ext,p}}{1 - N_{eff}\chi_{ext,p}} \\ &= \frac{\chi_{ext,c}/\phi}{1 - N_{eff}\chi_{ext,c}/\phi}, \end{aligned} \tag{3}$$

where $\chi_{ext,p}$ is the external susceptibility of the particles, $\chi_{ext,c}$ is the external susceptibility of the composite, and $\chi_{ext,p} = \chi_{ext,c}/\phi$.

2) DEMAGNETIZING FACTORS FOR SUPERPARAMAGNETS

In a composite (e.g., disk) of *superparamagnetic* particles, each particle acts as a macrospin, so the correct analogy is a uniform paramagnetic disk, not a composite of paramagnetic particles. As insightfully described in the Denmark model for composites of single-domain ferromagnetic and superparamagnetic particles [14], [15], *the only relevant demagnetizing factor is that of the composite*.[5] The composite's demagnetizing field is $H_d = -N_cM_c$, where the magnetization M_c is the magnetic moment of the composite m (originating from the particles) divided by the volume of the composite V (the total particle volume V_p divided by the filling fraction ϕ).

[1] Traditionally, magnetic viscosity occurs when relaxation times are on the order of experimental times [2]. However, as discussed in Section IV, magnetic viscosity actually persists over a much larger range of measurement times. Magnetic viscosity is not related to field-dependent ferrofluid viscosity measured in units of pascal seconds.

[2] As noted by Bean and Livingston [2] and Lin [7], the initial susceptibility for distributions of randomly oriented particles with shape or cubic magnetocrystalline anisotropy will be the same as for isotropic particles.

[3] In Casimir's [11] often-overlooked monograph, p. 11, the words "body" and "powder" refer to the composite; the word "crystals" refers to the particles, taken to be spherical. Casimir's symbols $H_0, f, V, M, J_a, J, H_a, H, \alpha_e$ refer here to $H_{ext}, \phi, V, m, M_c, M_p, H_{int,c}, H_{int,p}, N_c$. Casimir's monograph informed the often-cited article by Bleaney and Hull [13]. The derivation by Skomski et al. [12] does not make reference to these prior works.

[4] This is Casimir's [11] Eq. (1) on p. 11. Note that N_{eff} multiplies the magnetization of the particles M_p, not that of the composite.

[5] An implication, as described by Zambach et al. [14], [15], is that very large particle susceptibilities are obtainable for superparamagnetic nanoparticles.

The internal field of the composite is:[6]

$$H_{int,c} = H_{ext} - N_c M_c = H_{ext} - N_c \frac{m}{V}$$
$$= H_{ext} - N_c \frac{\phi m}{V_p} = H_{ext} - N_c \phi M_p. \quad (4)$$

The internal susceptibility of the composite is

$$\chi_{int,c} = \frac{M_c}{H_{int,c}} = \frac{M_c}{H_{ext} - N_c M_c} = \frac{\chi_{ext,c}}{1 - N_c \chi_{ext,c}}, \quad (5)$$

where $\chi_{ext,c}$ is the external susceptibility of the composite. If one recalls that $M_p = M_c/\phi$, $\chi_{ext,p} = \chi_{ext,c}/\phi$, and $\chi_{int,p} = \chi_{int,c}/\phi$, then the internal susceptibility of the particles, the subject of interest, is

$$\chi_{int,p} = \frac{M_p}{H_{int,c}} = \frac{M_p}{H_{ext} - N_c \phi M_p} = \frac{\chi_{ext,p}}{1 - N_c \phi \chi_{ext,p}}. \quad (6)$$

By comparison to composites of *paramagnetic* particles above, $N_{eff} = N_c \phi$. The particle demagnetizing factor exists (nominally equal to 1/3), but it does not enter into the calculation of internal susceptibility because of the paramagnetic macrospin nature of superparamagnetism.

A demagnetizing-factor correction for susceptibility is needed only if N_c, ϕ, and $\chi_{ext,p}$ are non-negligible. For toroidal specimens of single-domain particles in azimuthal field measured here, $N_c = 0$, so $\chi_{int,p} = \chi_{ext,p}$.

D. FIGURES OF MERIT

The suitability of magnetic nanoparticles for an intended application may be quantified on the basis of figures of merit. Figures of merit for intrinsic properties should be independent of extrinsic properties, such as particle concentration. Assumptions made in the calculation of derived quantities should be explicit.

Three physical figures of merit come to mind: particle size distribution (usually a narrow distribution is better), particle phase purity (for example, all magnetite rather than a mixture of magnetite and maghemite), and particle crystal purity (single-crystal particles with no surface ''dead'' layer or surface spin canting). The specimens used here have none of these, which is of secondary importance. The purpose is to describe analytic methods and their agreement with experiment for typical commercial nanoparticle solutions.

A figure of merit for magnetic nanoparticles might be their magnetic moment divided by their volume: the particle magnetization. This could be determined from a measurement of saturation moment if the total volume of particles were known. Alternatively, the magnetic moment per particle may be deduced from classic Langevin paramagnetism. Ideally, the magnetic moment per particle volume of high-quality nanoparticles with phase and crystal purity would approximate the magnetization of the bulk material.

However, magnetic moment and magnetization do not capture the particles' time-dependent response. Hysteresis loops as a function of frequency can achieve this at audio frequencies [16]. Complex susceptibility, as measured here at radio frequencies, is especially revealing because it quantifies both dispersion and losses. The intrinsic complex susceptibility of a composite divided by its particle concentration serves as a good figure of merit, whereas magnetic susceptibility alone is inadequate for a composite because it depends on the number of particles in a specimen and the volume of each particle. Another magnetic figure of merit at radio frequencies might be the loss tangent: the ratio of the imaginary and real parts of complex permeability. As shown below, the imaginary part of complex susceptibility scaled by the particle concentration may be a superior metric.

II. ANALYSIS

A. METHOD

The goal of this work is to show how the susceptibility of assemblies of particles in any concentration — in liquid or a dry matrix — at a single temperature can predict the intrinsic susceptibility and thus can be used to compare particle quality across batches and laboratories. Particle size distribution, phase purity, and crystal purity mentioned above would be characterized independently. Particle size distributions are often measured using transmission electron microscopy, dynamic light scattering, or magneto-granulometry — the analysis of curves of magnetization versus magnetic field [8], [17], [18], [19], [20], [21], [22]. As described by Bean and Jacobs [8] and Becker [17], larger particles may be quantified by the initial slope of the magnetization curve and smaller particles by the approach to saturation. In the model by Chantrell et al. [19], the particle size distribution may be calculated from the initial susceptibility, the saturation magnetization, and the dependence of magnetization on the reciprocal of the applied field.

The universal approach has been to first posit the value of the intrinsic susceptibility of superparamagnetic nanoparticles — the Langevin susceptibility — and then use models to calculate what would be the susceptibility of interacting particles. The inverse approach is used here: The intrinsic susceptibility is derived from the measured susceptibility of interacting particles by employing three relatively simple but proven models for superparamagnetism: the Weiss molecular-field model, of which the Lorentz cavity-field model is a special case; the Onsager model; and the modified mean-field model.

As described below, the phenomenological *Weiss molecular-field* model considers the effect of neighboring magnetic moments on an individual moment. In addition to an applied field, the local field provided by the neighbors is assumed to be equal to the magnetization of the material times a factor of γ. It is manifest in the well-known Curie-Weiss law for paramagnetism. The *Lorentz* approach, originally developed for dielectrics, considers the local field experienced by a magnetic moment within a spherical hole in a uniform magnetic medium to be equal to the magnetization times the cavity's demagnetizing factor of 1/3. This happens

[6]Casimir [11] anticipates this equation on p. 11 after the words, ''will be given by.''

to be mathematically equivalent to $\gamma = 1/3$ in the Weiss model, so one may treat them together. As an extension of Lorentz's treatment of polarization, *Onsager* considered randomly oriented permanent dipole moments for the calculation of local fields. The *modified mean-field* model considers the local field experienced by a magnetic moment to be equal to one third of the ideal Langevin magnetization, calculated from the Langevin susceptibility, in addition to the applied field. Its elaborate calculation belies its conceptual simplicity. As shown below, it gives values of intrinsic susceptibility that are rather independent of particle concentration, within experimental error.

Many of the references cited below justify the use of each of these models but point out their failure to be universally applicable. For data reports and interlaboratory comparisons, specification of the model used to calculate intrinsic susceptibilities would be advisable, with no implied claim of absolute accuracy.

The susceptibilities in the interaction models were originally developed for paramagnetism but were later extended to superparamagnetism. Here, the susceptibilities in the interaction equations are further treated as complex variables that are then used to obtain complex intrinsic susceptibilities. Once a material's complex intrinsic susceptibility is known, the complex susceptibility of any concentration can be predicted from one of the three models.

As shown below, the particles' radio-frequency susceptibility has real (inductive) and imaginary (resistive) parts. The case is made that the model for superparamagnetism can be extended to radio frequencies above the blocking frequency, where magnetic viscosity is measurable. Certainly, the three interaction models can be applied to the absolute value of susceptibility, which is immune to the phase lags that arise from magnetic viscosity.

The analysis may be extended further by treating the real and imaginary parts of susceptibility as valid characteristics of viscous superparamagnetic particles. The conjecture is that viscous nanoparticles retain their monodomain, thermally activated nature, although they do not satisfy the classic criteria for superparamagnetism.

Thus, the complex radio-frequency susceptibility of interacting magnetic nanoparticles is modeled using complex renditions of superparamagnetic interaction models to predict the particles' intrinsic complex susceptibility.

B. LANGEVIN MODEL

The symbol χ_0 denotes the intrinsic (Langevin) susceptibility of noninteracting particles, and the symbol χ refers to the measured susceptibility. If the interaction follows the Weiss molecular-field model, then $\chi \equiv \chi_W$; if the Onsager model, then $\chi \equiv \chi_{On}$; if the modified mean-field model, then $\chi \equiv \chi_m$. The interactions are assumed to be dipolar. (Exchange interactions could apply if particles were aggregated such that they shared crystallographic boundaries. Particles coated with polymers or nonmagnetic shells and measurement in low fields inhibit agglomeration.) If there were no interactions, then $\chi \equiv \chi_0$. Because χ is a complex quantity,[7] $\chi = \chi' - i\chi''$, so is χ_0 calculated from the models: $\chi_0 = \chi_0' - i\chi_0''$.

The classic Langevin [23] theory for magnetization as a function of field for paramagnetism is

$$M = nm\left(\coth\alpha - \frac{1}{\alpha}\right) = nm\left(\frac{\alpha}{3} - \frac{\alpha^3}{45} + \frac{2\alpha^5}{945} - \ldots\right), \quad (7)$$

$$\alpha = \frac{\mu_0 mH}{kT}, \quad (8)$$

where M is the magnetic moment per volume, n is the number of molecules (i.e., particles) per volume, m is the magnetic moment per molecule (particle), μ_0 is the permeability of vacuum, H is the applied magnetic field (which, for toroids in azimuthal field, does not need to be corrected for demagnetizing field), k is the Boltzmann constant, and T is the absolute temperature.

In the limit $H \to 0$,

$$\chi_0 = \frac{\partial M}{\partial H} = \frac{\mu_0 nm^2}{3kT} = \frac{C}{T}, \quad (9)$$

where χ_0 is the Langevin susceptibility of non-interacting particles and C is the Curie constant.

In Eqs. (7) and (9), $n = N/V = V_p/V_{1p}V = \phi/V_{1p}$, where N is the total number of particles in a solution or solid matrix, V is the total volume, V_p is the total particle volume, V_{1p} is the volume of a single particle, and ϕ is the filling fraction of the particles in a solution or solid matrix.

If M and χ_0 were based on total particle volume instead of composite volume, one would have $n_p = N/V_p = 1/V_{1p}$. That is, $n_p = n/\phi$. For this article, M and χ are measured and M/ϕ (particle magnetization) and χ_0/ϕ are reported.

C. WEISS AND LORENTZ MODELS

Modifications to the Langevin function to account for particle dipolar interactions will allow χ_0 to be calculated in terms of measured susceptibilities. The phenomenological Weiss molecular-field model [24], [25] accounts for the net effect of neighboring magnetic moments on an individual moment:

$$H_W = H + \gamma M, \quad (10)$$

where H_W is the Weiss field and γ is the molecular field parameter. In this case,

$$\alpha = \frac{\mu_0 m\,(H + \gamma M)}{kT} \quad (11)$$

in the Langevin equation. In the low-field limit, the equation for M is now

$$M = \frac{\mu_0 nm^2}{3kT}(H + \gamma M), \quad (12)$$

$$(1 - \gamma\chi_0)\,M = \chi_0 H, \quad (13)$$

[7] The negative sign indicates that the magnetization lags the magnetic field and that χ_0'' is positive: $H = H_0 e^{i\omega t}$, $M = M_0 e^{i(\omega t - \varphi)}$, $\chi = M/H = (M_0/H_0)e^{-i\varphi} = (M_0/H_0)\cos\varphi - i(M_0/H_0)\sin\varphi = \chi' - i\chi''$.

and the Weiss susceptibility, as given after the words, "and hence," on page 59 of the monograph by Casimir [11] for the particular Lorentz case $\gamma = 1/3$, is more generally

$$\chi_W = \frac{\partial M}{\partial H} = \frac{\chi_0}{1 - \gamma \chi_0}, \tag{14}$$

which can be written as

$$\chi_W = \frac{C/T}{1 - \gamma C/T} = \frac{C}{T - \gamma C} = \frac{C}{T - \theta}, \tag{15}$$

where $\theta = \gamma C$ is the Weiss constant (superparamagnetic Curie temperature). Positive values of θ, and therefore γ, indicate that the molecular field supports the applied field, whereas negative values indicate that the molecular field opposes the applied field.

If the Weiss molecular field is applicable in a specimen, then χ_W is what is measured (note that $\chi_W = \partial M/\partial H \neq \partial M/\partial H_W$) and χ_0 may be calculated from Eq. (14):

$$\chi_0 = \frac{\chi_W}{1 + \gamma \chi_W}. \tag{16}$$

The intrinsic susceptibility of the particles χ_0 is smaller than their measured susceptibility χ_W because the effective field to which they are exposed in the measurement is larger than just the applied field.

For the linear case $\chi_W = \partial M/\partial H = M/H$, Eq. (16) can be written as

$$\chi_0 = \chi_W H/H_W, \tag{17}$$

which is apparent upon substituting Eq. (10).

At high frequencies, the magnetic moment will lag the magnetic field, resulting in complex susceptibilities. In the complex Langevin model of noninteracting particles,

$$\chi_0 = \chi_0' - i\chi_0''. \tag{18}$$

In the complex Weiss model,

$$\chi_W = \chi_W' - i\chi_W'', \tag{19}$$

and substitution into Eq. (16) gives, after separation of real and imaginary parts,

$$\begin{aligned} \chi_0 &= \chi_0' - i\chi_0'' \\ &= \left[\frac{\chi_W' + \gamma\left(\chi_W'^2 + \chi_W''^2\right)}{\left(\gamma\chi_W' + 1\right)^2 + \left(\gamma\chi_W''\right)^2} \right] \\ &\quad - i\left[\frac{\chi_W''}{\left(\gamma\chi_W' + 1\right)^2 + \left(\gamma\chi_W''\right)^2} \right]. \end{aligned} \tag{20}$$

A calculation of $|\chi_0| = \left|\chi_0' - i\chi_0''\right| = \sqrt{\chi_0'^2 + \chi_0''^2}$ restores Eq. (16). Thus, accounting for particle interactions changes the magnitude and phase of the calculated intrinsic susceptibility compared to the measured values (χ_W' and χ_W'' in this case).

To obtain χ_0 from the measured χ_W, an estimate is needed for γ. One could use $\gamma = 1/3$, as in the Lorentz [26] cavity-field approximation, or one could obtain γ from the slope and the temperature-axis intercept of χ_W^{-1} vs. T [27], although it would negate the advantage of measurement at a single temperature. For $\gamma = 0$ (no particle interactions), $\chi_0 = \chi_W' - i\chi_W''$, as expected.

The non-complex magnetic moment m, if used as a figure of merit, would be computed from the modulus $|\chi_0| = |\chi_0' - i\chi_0''| = \sqrt{\chi_0'^2 + \chi_0''^2}$ and Eq. (9).[8]

A possible figure of merit at a given frequency is the loss tangent (dissipation factor), where small values are better for electronic applications and large values are better for heating applications:

$$\tan\delta = \frac{\mu_r''}{\mu_r'} = \frac{\chi_0''}{1 + \chi_0'}, \tag{21}$$

where and μ_r' are μ_r'' are the real and imaginary parts of the relative permeability. In terms of the measured susceptibilities in the Weiss model, χ_0' and χ_0'' may be calculated from Eq. (20).

Weiss introduced the molecular field [24] to account for interactions in paramagnetic materials and, together with his concept of magnetic domains ("crystals"), to explain bulk ferromagnetism. The latter was superseded by Heisenberg's electron interchange interaction: the exchange interaction. It is above the Curie temperature where the molecular field has found application in ferromagnetism. The molecular-field model was applied to interacting superparamagnetic clusters in partially ordered alloys by Goldfarb and Patton [27] and to superparamagnetic particles by O'Grady et al. [28] and others cited by Pshenichnikov [29].

Equation (16) shows that measured susceptibility χ_W is reduced to obtain the intrinsic susceptibility χ_0. The form of the equation is reminiscent of the equation to correct external susceptibility χ_{ext} by the demagnetizing factor N to obtain the internal susceptibility χ_{int} characteristic of a magnetic material:

$$\chi_{int} = \frac{\chi_{ext}}{1 - N\chi_{ext}}. \tag{22}$$

For finite geometries, such as cylinders or disks instead of toroids, demagnetizing factor corrections must be made. In that case, plots of χ_{int}^{-1} vs. T are shifted vertically down from χ_{ext}^{-1} vs. T by N:

$$\chi_{int}^{-1} = \chi_{ext}^{-1} - N. \tag{23}$$

Extrapolations of pseudo-linear χ_{ext}^{-1} vs. T above the blocking temperature to $\chi_{ext}^{-1} = 0$ at a temperature $\theta <$

[8] When comparing susceptibilities from the complex and non-complex Weiss models, one may note that $|\chi_0/(1+\gamma\chi_0)| > |\chi_0|/(1+\gamma|\chi_0|)$. The left side refers to χ_0 obtained from the complex Weiss model, Eq. (20). The right side refers to χ_0 obtained from the non-complex Weiss calculation, Eq. (16). The left and right sides are almost equal for $\chi_0' \gg \chi_0''$ or $\chi_0'' \to 0$ or $\gamma \to 0$. Numerical values calculated using the left side are those presented in this article. As a hypothetical example, measured $\chi_0' = 2$, measured $\chi_0'' = 1$; in the Weiss model with $\gamma = 1/3$, calculated $|\chi_0| = 1.3156$ from Eq. (20) whereas calculated $|\chi_0| = 1.2812$ from Eq. (16). (In the Langevin model, calculated $|\chi_0| = \sqrt{5} = 2.2361$.) Comparable considerations apply to the Onsager and modified mean-field models.

0 often will result in actual $\theta > 0$ for χ_{int}^{-1} vs. T after the demagnetizing factor correction. The effect may be significant for superparamagnetic nanoparticles that have large magnetization at low fields, and therefore small reciprocal susceptibilities compared to N, such as those of iron, magnetite, and maghemite. If susceptibility is based on particle volume instead of composite volume, then, from Eq. (6),

$$\chi_{int,p}^{-1} = \chi_{ext,p}^{-1} - N_c\phi. \tag{24}$$

A shift will be apparent only if ϕ is large, which is consistent with significant dipolar interactions in the molecular-field model. Such demagnetizing factor corrections are rarely performed because authors often calculate mass susceptibility instead of volume susceptibility or plot susceptibility in arbitrary units. This could be the reason for disparate reports of negative values of θ for interacting superparamagnetic particles [28], [30], [31], [32], [33]. The point is that the Weiss molecular field is usually positive, not negative, and the net interparticle interaction due to long-range dipolar interactions usually reinforces the applied field. That said, one cannot discount the possibility that some particles are oppositely aligned with respect to an applied field and lateral nearest neighbors.

The clearest evidence in the present work for positive values of θ at low measurement fields is the excessive Langevin susceptibility in concentrated solutions when interactions are not considered compared to the Weiss correction. That is, the Langevin model does not acknowledge the positive molecular field that adds to the applied field to give a larger susceptibility than expected.

D. ONSAGER MODEL

Onsager [34] modified the Lorentz model [26] for polar molecules, which are here analogous to superparamagnetic particles, by including a "reaction field." With that modification, the effect of the molecular field on a particle does not include the effect that particle has on the orientation of nearby particles.

According to Onsager,[9] as formulated by Casimir [11], the effective field H_{On} in a measurement is related to the applied field H,

$$H_{On} = \frac{3\chi_{On}+3}{2\chi_{On}+3}H. \tag{25}$$

Similar to above for χ_W,

$$\chi_{On} = \frac{\partial M}{\partial H}, \tag{26}$$

and as in Eq. (17) for the Weiss model, in the linear case,

$$\chi_0 = \frac{\chi_{On}H}{H_{On}}, \tag{27}$$

which yields

$$\chi_0 = \frac{\chi_{On}\,(2\chi_{On}+3)}{3\chi_{On}+3}. \tag{28}$$

If one wanted an expression for χ_{On} in terms of χ_0, to parallel Eq. (14), Eq. (28) can be arranged to give

$$\chi_{On} = \frac{3}{4}\left(\chi_0 + \sqrt{\chi_0^2 + 2\chi_0/3 + 1} - 1\right), \tag{29}$$

which appears in different visual form after the words, "and the solution is," on page 59 of Casimir's [11] monograph.

Similar to the above treatment of the Weiss model, the measured χ_{On} is considered to be complex,

$$\chi_{On} = \chi'_{On} - i\chi''_{On}. \tag{30}$$

Substitution into Eq. (28) gives

$$\begin{aligned}\chi_0 &= \chi'_0 - i\chi''_0 \\ &= \left\{\frac{\chi'_{On}\left(2\chi'^2_{On}+5\chi'_{On}+3\right)+\chi''^2_{On}\left(2\chi'_{On}+1\right)}{3\left[\left(\chi'_{On}+1\right)^2+\chi''^2_{On}\right]}\right\} \\ &\quad - i\left\{\frac{\chi''_{On}\left(2\chi'^2_{On}+4\chi'_{On}+2\chi''^2_{On}+3\right)}{3\left[\left(\chi'_{On}+1\right)^2+\chi''^2_{On}\right]}\right\}.\end{aligned} \tag{31}$$

A calculation of $|\chi_0| = \left|\chi'_0 - i\chi''_0\right| = \sqrt{\chi'^2_0 + \chi''^2_0}$ returns Eq. (28).

The applicability of the Lorentz and Onsager models is discussed in the monograph by Casimir [11],[10] the seminal article by Bean and Livingston [2], and in more recent work by Dormann et al. [36].

E. MODIFIED MEAN-FIELD MODEL

The modified mean-field model of Pshenichnikov et al. [37], discussed by Lebedev et al. [38], follows the development for the Weiss model except that the effective field H_m is now a function of the Langevin magnetization $M_L = \chi_0 H$:

$$H_m = H + \frac{M_L}{3}, \tag{32}$$

$$M = \frac{\mu_0 nm^2}{3kT}(H + \frac{M_L}{3}), \tag{33}$$

$$\chi_m = \frac{\partial M}{\partial H} = \chi_0(1 + \frac{\chi_0}{3}). \tag{34}$$

If the modified mean-field theory applies, then χ_m is measured and χ_0, the ideal Langevin susceptibility of non-interacting particles, may be calculated. From Eq. (34),

$$\chi_0 = \frac{3}{2}(\sqrt{4\chi_m/3 + 1} - 1). \tag{35}$$

[9] In his acclaimed article [34], Onsager derived expressions for the effective electric field G in terms of the dielectric constant ϵ and the applied electric field E : $G = [3\epsilon/(2\epsilon+1)]\,E$. Onsager's symbols E, G, ϵ correspond to $H, H_{On}, (\chi_{On}+1)$ here. As explained by Frank [35], Onsager's internal refractive index n may be taken to be unity.

[10] In Casimir's [11] analysis of the Onsager model, pp. 57–60, his symbols H, H_i, χ_0, χ correspond to $H, H_{On}, \chi_0, \chi_{On}$ here. Casimir concentrated on the predicted χ_{On} as a function of known χ_0 whereas, here, predicted complex χ_0 is calculated as a function of measured complex χ_{On}. Casimir also offered corrections for demagnetizing factors, which are not needed here.

The measured χ_m is considered to be complex,

$$\chi_m = \chi_m' - i\chi_m'', \tag{36}$$

and substitution into Eq. (35) is complicated:

$$\begin{aligned}\chi_0 &= \chi_0' - i\chi_0'' \\ &= \left\{\frac{\sqrt{6}}{4}\left(x^2+y^2\right)^{1/4}\left[1+\left(1+\frac{y^2}{x^2}\right)^{-1/2}\right]^{1/2} - \frac{3}{2}\right\} \\ &\quad - i\left\{\frac{\sqrt{6}}{4}\left(x^2+y^2\right)^{1/4}\left[1-\left(1+\frac{y^2}{x^2}\right)^{-1/2}\right]^{1/2}\right\},\end{aligned} \tag{37}$$

where $x = 3+4\chi_m'$ and $y = 4\chi_m''$. Similar to case for the Weiss and Onsager models, a calculation of $|\chi_0| = \left|\chi_0' - i\chi_0''\right| = \sqrt{\chi_0'^2 + \chi_0''^2}$ recovers Eq. (35).

The three models are all based on average fields. They differ somewhat physically, but mostly they differ algebraically. Their relative utility is examined below.

III. MEASUREMENTS

A. MATERIALS

Ferrofluids were from the PBG series made by Ferrotec (USA) Corporation, Livermore, California. The fluids were composed of a black-brown mixture of $\gtrsim$80% magnetite (Fe_3O_4) and $\lesssim$20% maghemite (γ-Fe_2O_3) nanoparticles made by co-precipitation, coated with polyethylene glycol (PEG), and suspended in deionized water. (The aqueous co-precipitation of iron ions yields a broad range of particle sizes compared to the thermal decomposition of iron oleate precursors [39], [40].) The PEG coating maintains particle separation. Based on a particle diameter distribution provided by Ferrotec, the magnetic core diameters range from 4 nm to 17 nm. The mean particle diameter is 9.50 nm, and the standard deviation is 2.29 nm (Appendix A). In this work, the particles are referred to as 9.5 nm Fe_3O_4 particles.

Although the phase purity and size dispersion of this material might be unacceptable for some fundamental studies, they are satisfactory for most of the practical applications listed in Section I-A, as evidenced by their commercial use. For the measurements and analyses here, some approximations were required.

The particle filling fraction ϕ of the ferrofluids was calculated from the measured solution mass $\mathcal{M}$, the measured solution volume V, the nominal mass density of magnetite $\rho_p = 5170$ kg/m^3, and the density of water $\rho_w = 1000$ kg/m^3 at ambient temperature:

$$\phi = \frac{V_p}{V} = \frac{\mathcal{M} - V\rho_w}{V(\rho_p - \rho_w)}, \tag{38}$$

where V_p is the volume of all the particles.[11] The numerical density of particles n is equal to ϕ divided by the volume of a single particle V_{1p}.

Six stock solutions covered a range of calculated filling fractions between 0.19 and 0.05 (Table 1). Calculations of particle concentration were generally larger than the manufacturer's estimates. The calculated values were used in this study.

TABLE 1. Nominal and calculated particle concentrations ϕ of six ferrofluid solutions.

Filling Fraction ϕ	PBG 900	PBG 600	PBG 450	PBG 400	PBG 300	PBG 200
Nominal	0.177	0.118	0.088	0.079	0.059	0.039
Calculated	0.187	0.142	0.118	0.078	0.069	0.052

B. MEASUREMENT METHODS

A Mettler-Toledo AT 201 balance with 10 µg resolution was used for mass measurements to calculate particle filling fraction ϕ, Eq. (38).

Quasi-static magnetization–field loops were measured with a Lake Shore Cryotronics vibrating-sample magnetometer, model 8607, with a single-stage variable-temperature cryostat.[12] Specimens were frozen in zero field, away from the electromagnet, to prevent agglomeration of magnetized particles during high-field measurements. Hysteresis loops of magnetic moment as a function of field between ±1.6 MA/m were measured at temperatures no higher than 265 K to preserve the specimens' frozen state. Zero-field-cooled, field-cooled, and thermoremanent magnetic moment versus temperature were measured from 78 K to 265 K in small applied fields.

The permeabilities of ferrofluids of different particle concentrations in toroidal capsules were measured from 1 MHz to 1 GHz using the impedance-analyzer method based on a shorted coaxial transmission line described by Goldfarb and Bussey [41] and later offered commercially by Hewlett-Packard Company [42], [43]:

$$\mu_r' = 1 + \frac{2\pi\,\Delta L}{\mu_0 h \ln(b/a)}, \tag{39}$$

$$\mu_r'' = \frac{\Delta R}{\mu_0 f\ h \ln(b/a)}, \tag{40}$$

where μ_r' is the real part of relative permeability, μ_r'' is the imaginary part of relative permeability, μ_0 is the permeability

[11] Intermediate algebraic steps for the derivation of Eq. (38), where $\mathcal{M}_p$ is the total particle mass and $\mathcal{M}_w$ is the mass of water: $V_p = \mathcal{M}_p/\rho_p = (\mathcal{M} - \mathcal{M}_w)/\rho_p = (\mathcal{M} - V_w\rho_w)/\rho_p = \left[\mathcal{M} - (V - V_p)\,\rho_w\right]/\rho_p$. The density of the PEG particle coating, approximately 1130 kg/m^3, was taken to be the same as that of water.

[12] The uncertainty in magnetization due to random effects (e.g., magnetic field noise, variation in sample vibration amplitude) is estimated to be 1 %. The uncertainty due to systematic effects (e.g., magnetometer calibration, estimation of particle diameter, measurements and assumptions for calculation of filling fraction including the assumption that all particles are magnetite) is estimated to be 5 %.

of vacuum, ΔL and ΔR are the changes in inductance and resistance when the toroid is inserted in the measurement fixture, f is the frequency in hertz, h is the toroid height, and b and a are the toroid outer and inner diameters. As noted above, the toroidal geometry eliminates the need to consider demagnetizing factors.

Toroidal capsules consisted of two plastic polymer halves affixed with cyanoacrylate glue (Fig. 1). The top halves had two holes, one to receive the tip of a calibrated pipette, the other to serve as a vent. The pipette was calibrated using the mass of a dispensed aliquot of water. After filling with 0.8 mL of solution, the holes were sealed with a thermoplastic polymer adhesive. Given the outer and inner diameters of the liquid toroids, $b = 16.25$ mm and $a = 11.36$ mm based on the measured capsule dimensions, the toroid height was determined from the volume of solution. This defined the toroid dimensions for all specimens.

A Keysight E4991B impedance analyzer with material measurement firmware (option 002) was used with the large Keysight 16454A magnetic material test fixture, which is designed for toroids up to 20 mm outer diameter, down to 5 mm inner diameter, and up to 8.5 mm height.[13] Frequency was swept linearly from 1 MHz to 1 GHz and 128 scans were averaged for each measurement. The instrument directly reported values of μ_r' and μ_r'' based on the toroid dimensions.[14] (An alternative method for measurements at higher frequencies would be to use a vector network analyzer to measure scattering parameters [44], [45], [46].)

The test fixture creates a one-turn ''coil'' around the toroid cross section. The average azimuthal magnetic field strength H applied to the toroid, obtained from a calculation of flux density,[15] is

$$H = \frac{I}{2\pi\,(b/2 - a/2)\,h}\int_{a/2}^{b/2}\frac{h}{r}dr = I\frac{\ln(b/a)}{\pi\,(b-a)}. \qquad (41)$$

Although it does not enter into the data analysis, it is noteworthy that H is quite small, 0.23 A/m, based on the impedance analyzer's alternating output current I of 10 mA, outer toroid diameter $b = 16.25$ mm, and inner toroid diameter $a = 11.36$ mm. Measurements were made at ambient temperature, about 297 K.

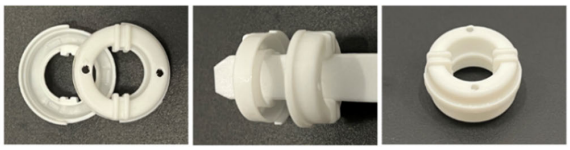

FIGURE 1. Toroidal capsules for liquid samples. Left: Plastic polymer halves. Center: Teflon guide strip to align the halves prior to application of glue. Right: Capsule halves snapped together and sealed. Solutions within the capsules had an outer toroid diameter $b = 16.25$ mm and an inner toroid diameter $a = 11.36$ mm.

C. QUASI-STATIC MAGNETIZATION–FIELD LOOPS

An expectation for superparamagnetism is a scaling of the curves of magnetization M versus field H for temperatures T above the blocking temperature T_b when they are plotted as M vs. H/T [2], [8], [17], [18]. However, perfect scaling is not obtained at high fields when a decrease in saturation magnetization with increasing temperature becomes evident, owing to insufficiently high Curie temperatures.

This is illustrated in Fig. 2 for the high-field portions of particle magnetization curves $M_p = m/V_p = M/\phi$ as functions of internal field scaled by temperature for a frozen sample of PBG 200, the ferrofluid with the smallest particle concentration and therefore the least interparticle interactions. The internal field was calculated by adjusting the applied field with a demagnetizing factor $N_c^{\perp}$ of 0.38 for a cylindrical solution specimen with a height-to-diameter ratio of 1.4 and approximately zero susceptibility in transverse field [47]: $H_{int} = H_{ext} - N_c^{\perp}M_c$, as in Eq. (4) for composites of superparamagnetic particles. Despite the accentuated differences in this amplified plot, the lower-temperature curves scale rather well.

For Fig. 2, particle magnetization was calculated as the magnetic moment divided by the total particle volume, which was calculated using Eq. (38) for a sample volume of 4.95×10^{-8} m^3 (a slight adjustment from the nominal 50 µL dispensed from a pipette in order to assure the same filling fraction ϕ for PBG 200 as in Table 1).

The low-field details of hysteresis loops cycled between ±80 kA/m in 42 s for different temperatures are shown in Fig. 3. The time between successive data points in Fig. 3 was 0.1 s. The 265 K curve is reversible. A tiny amount of hysteresis arises at 251 K (not shown to avoid clutter in the figure). The hysteresis increases with decreasing temperature. A linear fit to the 265 K curve between ±3 kA/m gives an initial susceptibility of 16, which is consistent with the radio-frequency susceptibility discussed below in the low-frequency limit.

A particle saturation magnetization $M_{p,s}$ of 328 kA/m was obtained from a linear extrapolation to zero of the 265 K magnetization vs. reciprocal field,[16] $M_p$vs.$1/H_{int}$,

[13] When the residual series inductance $L_{s,res}$ and resistance $R_{s,res}$ of the E4991B impedance analyzer's empty magnetic measurement fixture are compensated in permeability mode, the current system firmware (A.02.16) nulls $R_{s,res}$ but not $L_{s,res}$. If μ_r' were calculated under the mistaken assumption that measured L_s equals ΔL in Eq. (39), μ_r' would be too large by exactly unity (which is negligible for materials with high permeability), whereas measured R_s does equal ΔR in Eq. (40). Nevertheless, the values of μ_r' and μ_r'' reported in permeability mode are correct if the exact toroid dimensions are input after fixture compensation and before measurement.

[14] The uncertainty in the ratio of susceptibility to filling fraction at a given frequency due to random effects (e.g., instrument noise, repeatability of fixture short connection) is estimated to be 0.1. The uncertainty due to systematic effects (e.g., calibration of instruments, impedance compensation of measurement fixture, estimation of particle diameter, measurements and assumptions for calculation of filling fraction including the assumption that all particles are magnetite) is estimated to be 0.5.

[15] The same equation, without the h, is for the average field H external to a straight conductor carrying current I.

[16] Magnetite nanoparticles typically have saturation magnetizations below the 445 kA/m of bulk magnetite [48], which may be due to surface spin disorder [49], iron oxidation state [50], or crystal defects [51].

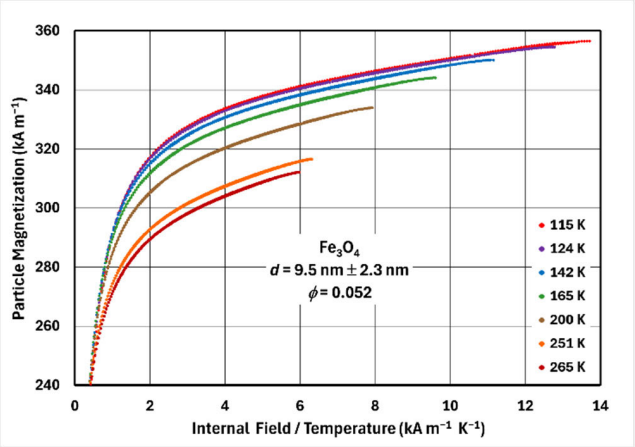

FIGURE 2. Magnetization versus internal field scaled by temperature for PBG 200 frozen in zero field. Aside from the expected decrease in saturation magnetization with increasing temperature, the scaling is satisfactory at low temperatures. The vertical axis scale does not begin at zero.

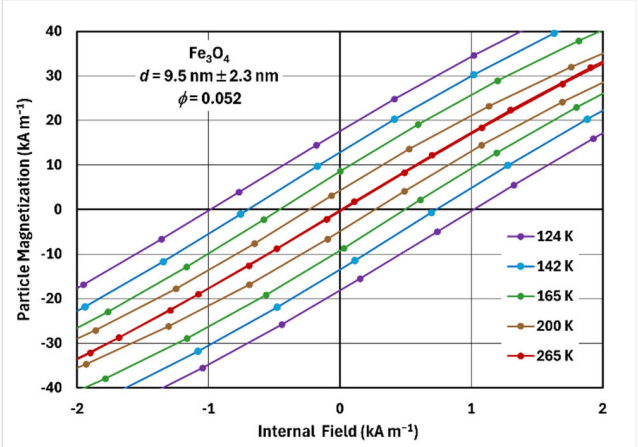

FIGURE 3. Details of the magnetization curves widely spaced in temperature. There is no measurable hysteresis at 265 K.

above 1 MA/m. This $M_{p,s}$ and a particle diameter of 9.5 nm give[17] a particle moment m of 1.47×10^{-19} A·m^2. (In Table 2 below, the moment per particle m is compared with m derived from $|\chi_0|$ at 297 K.) The reciprocal of the particle volume gives a numerical particle density n_p of 2.23×10^{-24} m^{-3}. (An explanation of n_p follows Eq. (9) above.) These values of m and n_p define the theoretical Langevin curve, Eqs. (7) and (8), plotted in Fig. 4 along with the experimental 265 K curve. The 265 K curve does not closely follow the Langevin function due to the distribution in particle sizes and their moments.

The high-field linear fit used to obtain the saturation magnetization of 328 kA/m at 265 K may also be used to find a $1/H_{int}$ axis intercept, $1/H_0$, of 12.7 m/MA. Together with the initial susceptibility of 16, the Chantrell et al. [19] model for a log-normal distribution of the diameters of noninteracting particles yields an unrealistic median diameter[18] of 14.8 nm. (Particle size distribution is discussed in Appendix A.) As pointed out by Chantrell et al. [19], as well as Bean and Jacobs [8] and Becker [17], for a distribution in particle sizes, the initial susceptibility is more sensitive to the larger particles, and the approach to saturation is more sensitive to the smaller particles. Indeed, a Langevin fit to the 265 K magnetization curve for a hypothetical particle diameter of 6 nm fits the high-field data (Fig. 4), and a hypothetical diameter of 13 nm fits the low-field data (inset, Fig. 4).

The usual method to obtain T_b for quasi-static measurements is from the peak (or below the peak [52]) in the curve of zero-field-cooled (ZFC) magnetization measured as a function of increasing temperature. For a sample of frozen PBG 200, a measurement field of 800 A/m, and a temperature sweep rate of 5 K/min, a broad peak — reflective of the distribution in particle sizes and the increase in energy barrier due to some dipolar interactions [53], [54], [55], [56] — is roughly centered at $T_b \approx 180$ K (Fig. 5). The zero-field-cooled curve is reminiscent of measurements by Nedelkoski et al. [57], where peaks and shoulders were attributed to structural defects. The slight increase in the ZFC curve above 120 K may be attributable to the well-known Verwey transition [58] in magnetite.[19] The field-cooled (FC) magnetization measured upon warming merges with the ZFC curve at 238 K. All the particles are superparamagnetic above this temperature for this measurement field and time.

D. RADIO-FREQUENCY MEASUREMENTS

Measured permeability and four calculated susceptibilities for the most concentrated solution, PBG 900, at 297 K are displayed in Figs. 6–10. The real and imaginary parts of complex susceptibility were obtained directly from the measured real and imaginary permeabilities as $\chi' = \mu' - 1$ and $\chi'' = \mu''$. If there were no interactions, these would be the intrinsic susceptibilities χ_0' and χ_0'' (Langevin model). Otherwise, χ_0' and χ_0'' are model-dependent according to Eqs. (20), (31), or (37). All susceptibilities are scaled by the measured filling fraction ϕ (Table 1). The lowest frequency plotted is 6 MHz. (The 1 MHz point was often spurious.)

Figure 11 compares the susceptibility moduli $|\chi_0|$ for the four models for the most concentrated solution, PBG 900. The relative position of the Weiss curve depends entirely

[17]This is the inverse of strategies to estimate particle size from the magnetization curve [17], [18], [19].

[18]The analysis by Chantrell et al. [19] assumes a log-normal volume distribution. For use with SI units, their Eq. (8) for median particle diameter requires an additional factor of $\mu_0^{-1/3}$. Their Eq. (7) for standard deviation refers to a fraction of the median diameter value.

[19]Verwey documented a sudden increase in magnetite's electrical resistance at 117 K upon cooling [59]. Verwey cited Weiss and Forrer [60] for their prior reporting of a sharp increase in magnetization, especially pronounced at low fields, with increasing temperature between 116 K and 120 K. Weiss and Forrer, in turn, credited Weiss's graduate student, Renger [61], for measuring an abrupt decrease in susceptibility (his symbol k) at low field (59 A/m) upon cooling between 140 K and 120 K. With decreasing temperature, the magnetocrystalline anisotropy constant K_1 of magnetite goes from negative to zero at the Verwey temperature [62].

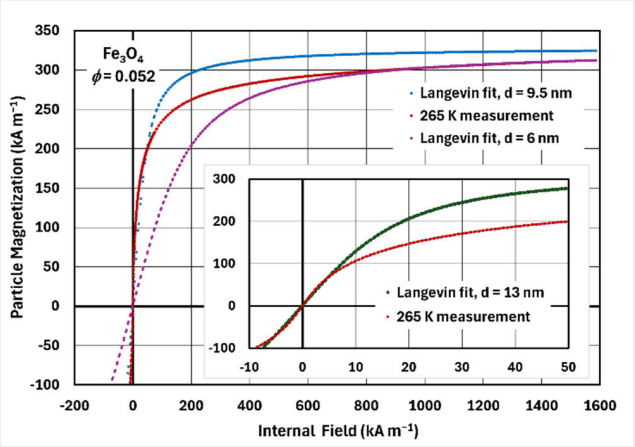

FIGURE 4. Langevin fits to the 265 K magnetization curve. A curve calculated using a particle diameter of 9.5 nm underestimates the magnetization at low fields and overestimates it at high fields. A diameter of 6 nm fits the data well at high fields but underestimates at low fields. A diameter of 13 nm fits the data at low fields but overestimates at high fields (inset).

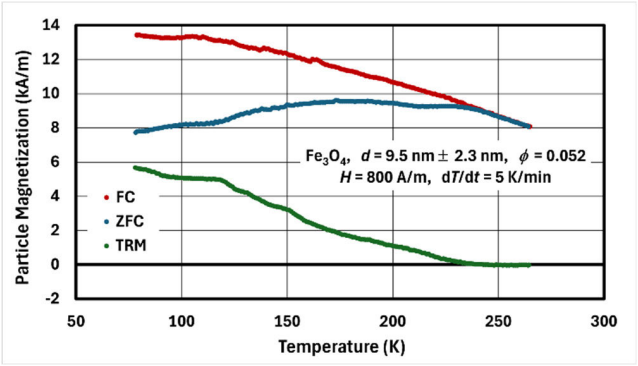

FIGURE 5. For PBG 200, field-cooled (FC), zero-field-cooled (ZFC), and thermoremanent (TRM) magnetization as functions of temperature increasing at a rate of 5 K/min for a measurement field of 800 A/m. The broad peak in the ZFC curve is indicative of the range of particle sizes and blocking temperatures. The FC and ZFC curves merge at 238 K, the blocking temperature of the largest particles. As expected, the difference between FC and ZFC curves closely approximates the measured TRM curve. The TRM curve dips very slightly below zero above 238 K owing to a negative offset in the zero-field setting of the electromagnet. The noise in the data arises from jitter in the applied field.

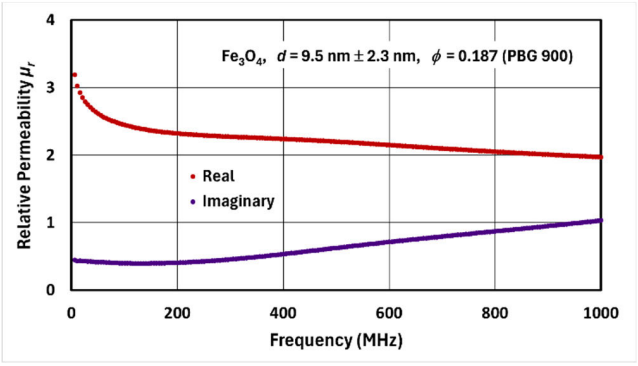

FIGURE 6. Real and imaginary parts of relative permeability of PBG 900 as functions of frequency at 297 K.

on the value chosen for γ. In this article, the Lorentz value $\gamma = 1/3$ is used.

The simple Langevin model, which assumes no particle interactions, overestimates the susceptibilities compared to the three interaction models. For all particle concentrations, the modified mean-field susceptibility is between the higher Onsager susceptibility and the lower Weiss susceptibility. If one took the traditional approach, in which the intrinsic Langevin susceptibility is taken to be known in advance and the susceptibility of interacting particles is calculated using different models, the trend would be the opposite: The Langevin susceptibility would be smaller than the model predictions, and the order of the model predictions would be reversed. This is illustrated by Fig. 2 in Pshenichnikov [29], Fig. 11 in Ivanov et al. [21], and Fig. 6 in Huang et al. [63].

As concentrations become more dilute, the susceptibilities from the different models converge. Figures 12 and 13 show comparisons of susceptibility moduli for PBG 600 and PBG 200.

Ideally, a favorable model should predict similar intrinsic susceptibilities regardless of the strength of the interactions. Figures 14–16 show $|\chi_0|$ at three representative frequencies for the different solution concentrations.

As expected, the simple Langevin model, which does not consider interactions, yields larger susceptibilities for all concentrations and frequencies (green circle symbols), with larger differences for higher concentrations. The modified mean-field model (blue rhombus symbols) is intermediate between the higher Onsager model predictions (red square symbols) and lower Weiss model predictions (indigo triangle symbols).

As a check for consistency, the magnetic moment per particle m may be calculated from $|\chi_0|$ and Eq. (9). Ranges of values are shown in Table 2 because $|\chi_0|$ varies with frequency. The values for the different models converge for the dilute solutions, as expected from the convergence of the susceptibility plots. The somewhat smaller values of $|\chi_0|/\phi$ for PBG 200 ($\phi = 0.052$) and PBG 450 ($\phi = 0.118$) in Figs. 14–16 and their slightly smaller magnetic moments summarized in Table 2 could be due to a higher percentage of maghemite in these two solutions. (All six samples came from different stock solutions from the manufacturer.)

To gauge losses, the loss tangent is often used: $\tan\delta = \mu_r''/\mu_r' = \chi_0''/(\chi_0' + 1)$. In the radio-frequency range, it is frequency-dependent and, for concentrated solutions, model-dependent. A large imaginary component, a measure of losses, is usually detrimental, but not always, as in hyperthermia applications. A large real component is usually beneficial, but not always, as when agglomeration must be avoided. The loss tangent blends the two. An alternative metric is simply the imaginary susceptibility scaled by the filling fraction: χ_0''/ϕ. The two are compared for three solutions in

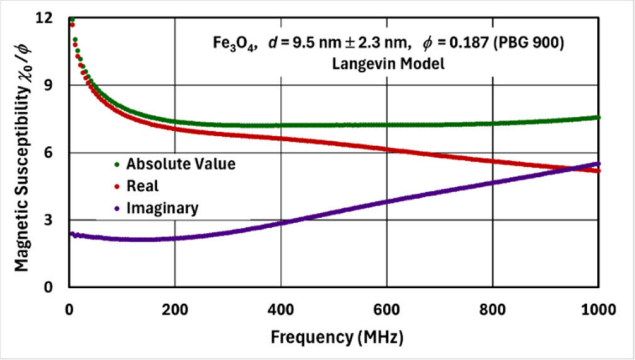

FIGURE 7. Real, imaginary, and modulus susceptibility scaled by filling fraction for PBG 900 as functions of frequency, Langevin model. Susceptibility was obtained directly from the data in Fig. 6 and a filling fraction of 0.187 (Table 1). The Langevin model assumes, incorrectly for PBG 900, that the particles do not interact.

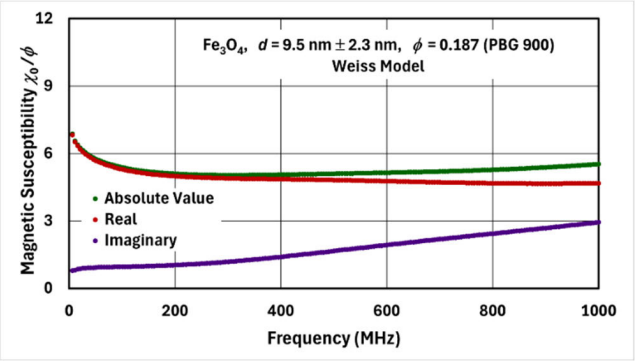

FIGURE 8. Real, imaginary, and modulus susceptibility scaled by filling fraction for PBG 900 as functions of frequency, Weiss model. The Weiss model accounts for particle interaction according to Eq. (20). For this calculation, γ was chosen to be 1/3, as in the Lorentz cavity-field model.

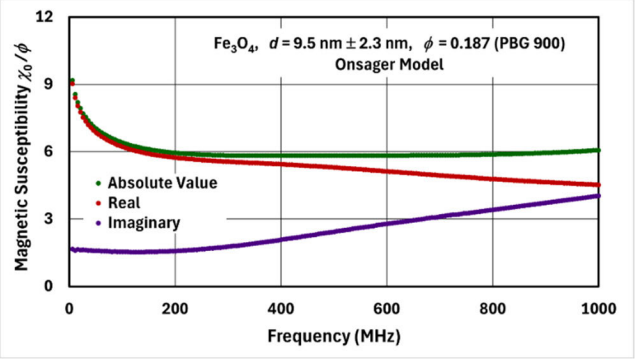

FIGURE 9. Real, imaginary, and modulus susceptibility scaled by filling fraction for PBG 900 as functions of frequency, Onsager model. The Onsager model accounts for particle interaction according to Eq. (31).

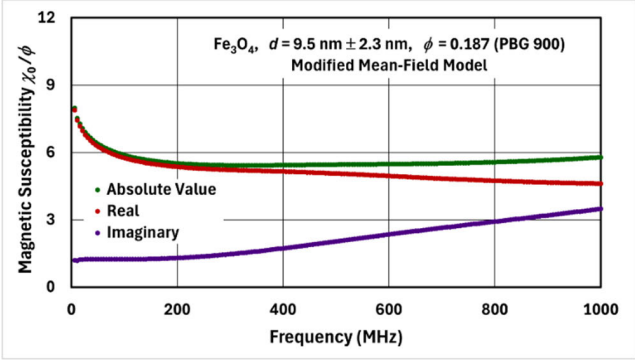

FIGURE 10. Real, imaginary, and modulus susceptibility scaled by filling fraction for PBG 900 as functions of frequency, modified mean-field model. The modified mean-field model accounts for particle interaction according to Eq. (37).

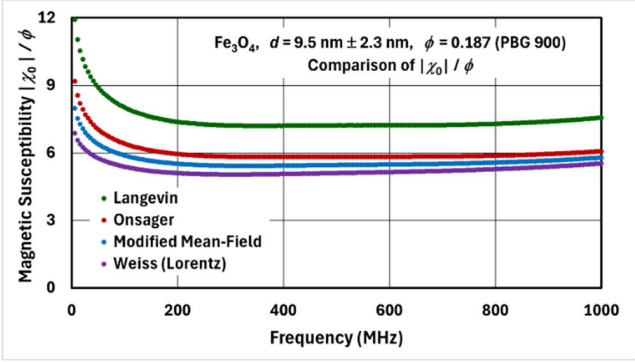

FIGURE 11. Comparison of susceptibility moduli scaled by filling fraction for PBG 900, the top green curves in Figs. 7–10.

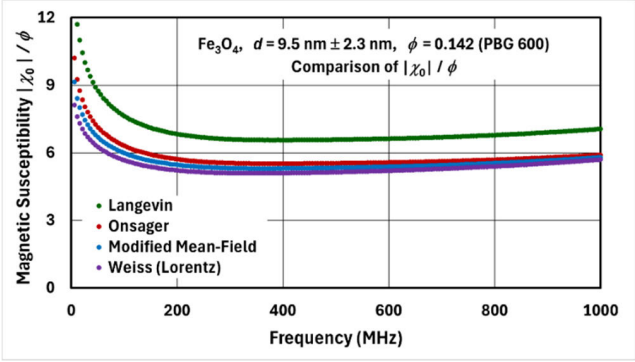

FIGURE 12. Comparison of susceptibility moduli scaled by filling fraction for PBG 600. The curves for the four models begin to converge.

Figs. 17–22. Particle loss tangent is calculated as $\tan\delta_p = (\chi_0''/\phi)/\left(1 + \chi_0'/\phi\right)$.

The interaction models serve as well for more concentrated solutions. As water evaporated from the PBG 900 capsule, the particle interactions increased. The smaller height of the toroid and the filling fraction could be calculated from the reduced mass of the capsule.[20] Figure 23 shows the susceptibility moduli for the different models for a filling fraction ϕ of 0.319. The differences in the models are accentuated compared to the original PBG 900 solution (Fig. 11). The curves

[20]To calculate the smaller solution volume V (and thus smaller toroid height) and increased filling fraction ϕ, use is made of Eq. (38), the conservation of the initially determined total particle volume V_p, the mass densities of the particles ρ_p and water ρ_w, and the smaller mass $\mathcal{M}$ of the solution after evaporation.

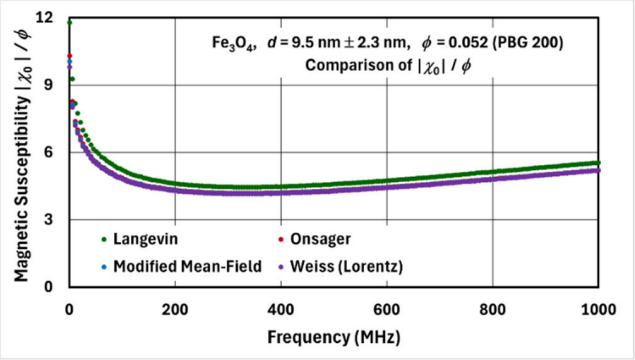

FIGURE 13. Comparison of susceptibility moduli scaled by filling fraction for PBG 200. The models converge for this dilute solution.

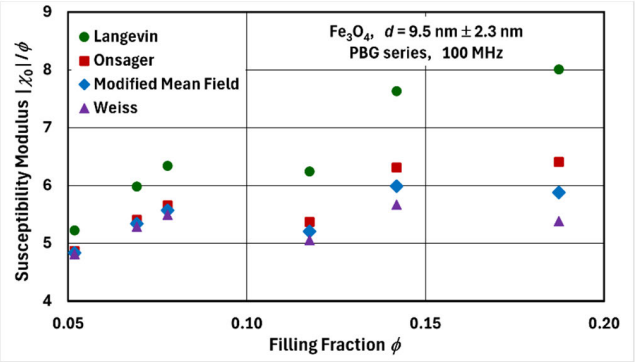

FIGURE 14. Modulus of susceptibility scaled by filling fraction at 100 MHz for all filling fractions.

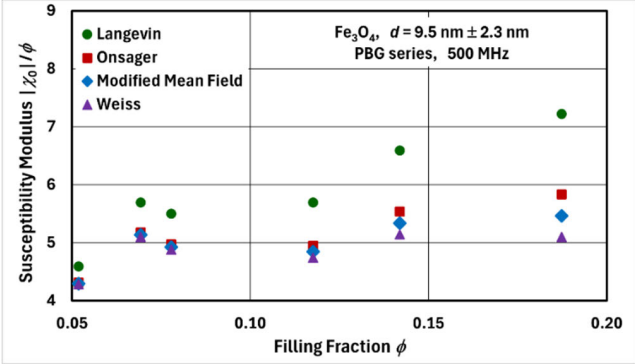

FIGURE 15. Modulus of susceptibility scaled by filling fraction at 500 MHz for all filling fractions.

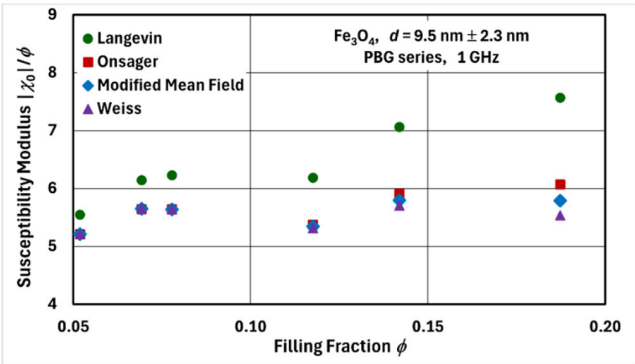

FIGURE 16. Modulus of susceptibility scaled by filling fraction at 1 GHz for all filling fractions.

for the different models are even more separated for dried powders (not shown).

IV. RELAXATION TIMES AND MAGNETIC VISCOSITY

This section makes use of many approximations and idealized equations. The intent is to show how concepts developed for ideal, monodisperse, superparamagnetic particles can provide qualitative context for the experimental measurements on polydisperse, commercial nanoparticle preparations.

A. BROWNIAN RELAXATION

According to the Debye equation [64], the rotational Brownian[21] relaxation time is $\tau_B = 3\eta V/kT$, where η is the dynamic viscosity of the medium (about 1 mPa·s for water), V is the particle hydrodynamic volume, k is the Boltzmann constant, and T is the absolute temperature. It is on the order of 0.4 µs for 10 nm diameter particles in water at ambient temperature if one neglects the effects of magnetic field strength, particle concentration, and particle coating. At frequencies of about 3 MHz and above, Brownian relaxation is suppressed, as it is at all frequencies in a solid matrix or in packed powders. For a larger hydrodynamic diameter of 40 nm, which is appropriate for 12 nm magnetite particles in solution [65], $\tau_B = 24$ µs, which corresponds to a Brownian relaxation frequency of 40 kHz. Brownian relaxation can be safely ignored above 1 MHz.

[21]Named after the Scottish botanist, Robert Brown (1773–1858), who famously described the random linear motion of pollen in water.

B. NÉEL RELAXATION AND BLOCKING TEMPERATURES

An important relaxation mechanism for magnetic nanoparticles is Néel relaxation. It cannot be ignored at radio frequencies. In the limit of zero applied field and no particle interaction, the Néel relaxation time is

$$\tau_N = \tau_0 \exp\left(\frac{K_{eff} V}{kT}\right), \tag{42}$$

where τ_0 is the attempt time, K_{eff} is an effective anisotropy constant, and V is the particle volume (referred to as V_{1p} above).[22] The Néel relaxation frequency $1/\tau_N$ could be called the "blocking frequency," a term that has gained currency since 2006 [68], [69], [70], [71]. The concept of blocking frequency at fixed temperature is analogous to that of blocking temperature at fixed frequency.

[22]Néel's formula is an Arrhenius equation, named for the Swedish physical chemist, Svante August Arrhenius (1859–1927), to describe the rate of a chemical reaction as a function of activation energy. A modification of Eq. (42) in which T is replaced by $(T - T_0)$, where T_0 is a constant, is known as the Vogel-Fulcher law. It has been used to account for dipolar interactions [66], [67].

TABLE 2. Magnetic moment per particle at 297 K calculated from susceptibility modulus over the range 1 MHz – 1 GHz. These may be compared to the value 1.47 × 10^{-19} A·m^2 based on the 265 K saturation particle magnetization of PBG 200 times the average particle volume.

Model	PBG 900	PBG 600	PBG 450	PBG 400	PBG 300	PBG 200
Langevin (10^{-19} A·m^2)	1.7–2.2	1.7–2.3	1.6–2.1	1.5–2.1	1.6–2.0	1.4–1.9
Onsager (10^{-19} A·m^2)	1.6–1.9	1.6–2.0	1.5–1.9	1.5–2.0	1.5–1.9	1.4–1.8
Modified Mean Field (10^{-19} A·m^2)	1.5–1.8	1.5–1.9	1.4–1.8	1.5–1.9	1.5–1.9	1.4–1.8
Weiss (10^{-19} A·m^2)	1.5–1.7	1.5–1.8	1.4–1.8	1.5–1.9	1.5–1.9	1.4–1.8

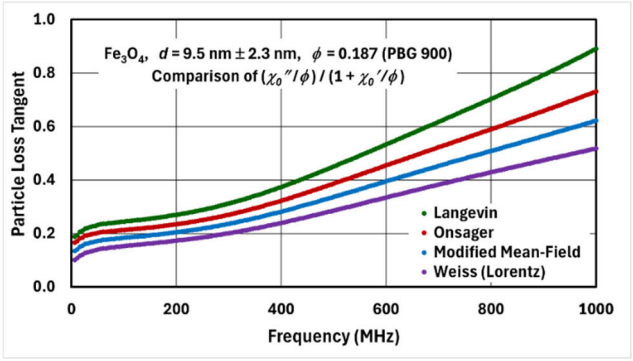

FIGURE 17. Particle loss tangent for PBG 900 for the different models.

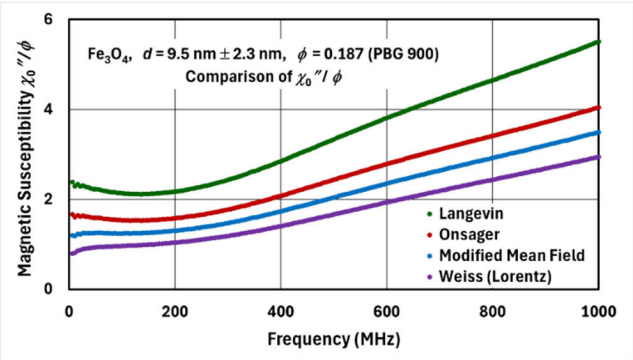

FIGURE 18. Imaginary part of susceptibility scaled by filling fraction for PBG 900 for the different models.

Proper interpretation of data for susceptibility as a function of frequency requires reasonable estimates of τ_0 and K_{eff}. They are elusive. The energy-barrier attempt time τ_0 is classically taken to be 1 ns [2], although estimates range from 1 ps to 1 ns [72], 10 ps to 0.1 ns [73], or 0.1 ns to 10 ns [74]. For illustrative purposes of this section, τ_0 is assumed to be 0.1 ns or 1 ns.

To model susceptibility as a function of frequency, one could refer to another Debye equation, the Debye relaxation

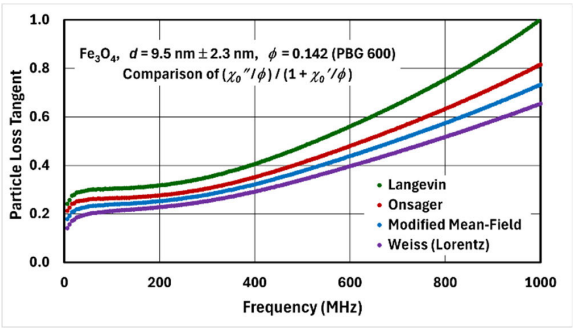

FIGURE 19. Particle loss tangent for PBG 600 for the different models.

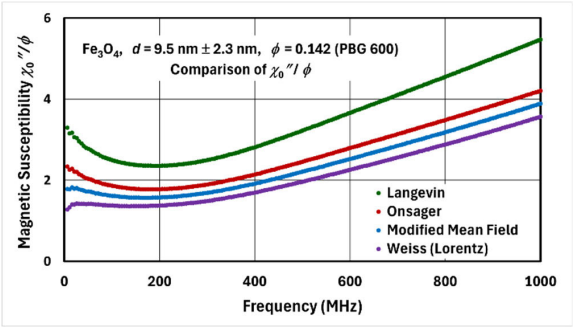

FIGURE 20. Imaginary part of susceptibility scaled by filling fraction for PBG 600 for the different models.

equation [64], [75], [76], [77], [78], [79],

$$\chi(\omega) = \frac{\chi_0}{(1 + i\omega\tau_N)} = \left[\frac{\chi_0}{(1 + \omega^2\tau_N^2)}\right] - i\left[\frac{\chi_0\omega\tau_N}{(1 + \omega^2\tau_N^2)}\right], \tag{43}$$

where χ_0 is the static Langevin susceptibility and ω is the angular frequency. A rigorous treatment would require monodisperse, noninteracting particles. It will not be attempted here.

1) MAGNETOCRYSTALLINE ANISOTROPY

For cubic crystals such as magnetite with ⟨111⟩ easy axes, negative magnetocrystalline anisotropy constant K_1, and neg-

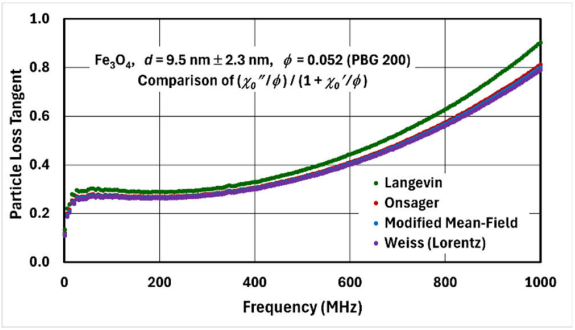

FIGURE 21. Particle loss tangent for PBG 200 for the different models.

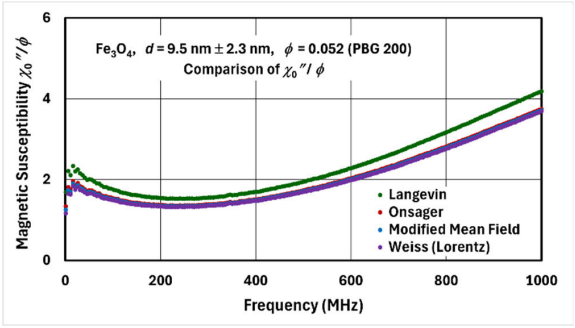

FIGURE 22. Imaginary part of susceptibility scaled by filling fraction for PBG 200 for the different models.

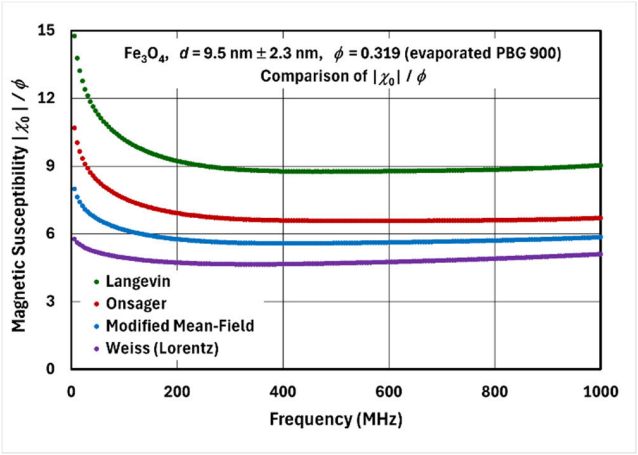

FIGURE 23. Susceptibility moduli scaled by filling fraction for evaporated PBG 900 with a filling fraction ϕ of 0.319. Compared to a ϕ of 0.187 (Fig. 11), the curves for the different models are more widely spaced. The modified mean-field curve is the least changed.

ligible K_2, the energy barrier is $K_{eff}V = -K_1V/12$ [2], [7], [36]. This ignores any shape or surface anisotropies.

For bulk magnetite at 300 K, $K_1 = -11$ kJ/m^3 [62], [80], [81] and thus $K_{eff} = 0.9$ kJ/m^3. For the present 9.5 nm particles at 297 K, with $\tau_0 = 0.1$ ns, and noting that $K_{eff}V < kT$, one would obtain $\tau_N = 0.11$ ns, equivalent to a Néel relaxation frequency $1/\tau_N$ of 9 GHz (summarized in Table 3), which is unreasonably high.

The blocking temperature T_b, below which magnetic viscosity appears, is a function of the measurement time $1/f$ [82], [83], [84], [85], [86], [87]. From Eq. (42),

$$T_b = \frac{K_{eff}V}{k\ln\left[(1/f)/\tau_0\right]}. \tag{44}$$

However, one would obtain unrealistically small values of T_b for measurements at the radio frequencies of the susceptibility measurements here, regardless of whether $\tau_0 = 0.1$ ns or $\tau_0 = 1$ ns (summarized in Table 3). Magnetocrystalline anisotropy alone does not give good estimates of blocking frequency at fixed temperature or blocking temperature at fixed frequency.

2) LARGER ANISOTROPIES

Compared to bulk crystals, the effective anisotropy constant K_{eff} is larger in magnetite nanoparticles, where surface anisotropy due to crystalline defects may be important. (For the idealized spherical particles considered here, one may ignore shape anisotropy.) Rosensweig [79] cited a range[23] from 23 kJ/m^3 to 41 kJ/m^3 for 10 nm magnetite particles. Ota and Takemura [65] estimated 15 kJ/m^3 to 18 kJ/m^3 for 12 nm particles. El-Hilo et al. [89] measured about 50 kJ/m^3 for 8 nm particles. Li et al. [90] calculated 16 kJ/m^3 for 8 nm particles. Moya et al. [56] fit 31 kJ/m^3 for 5.3 nm particles. Hadadian et al. [51] gave a range of 19 kJ/m^3 to 32 kJ/m^3 for 11 nm to 8 nm particles. Cabrera et al. [91] fit 26 kJ/m^3 for 12 nm iron oxide particles.

If one used $K_{eff} = 36$ kJ/m^3 for the present 9.5 nm particles at 297 K, with $\tau_0 = 0.1$ ns, and noting that $K_{eff}V > kT$, one would obtain $\tau_N = 5.1$ ns, equivalent to a Néel relaxation frequency $1/\tau_N = 194$ MHz (summarized in Table 3), still too high to account for the losses in the megahertz range. One could calculate values of $T_b = 127$ K for measurements at $f = 1$ MHz, $T_b = 170$ K at $f = 10$ MHz, $T_b = 254$ K at $f = 100$ MHz, and $T_b = 508$ K at $f = 1$ GHz. However, from the lossy radio-frequency measurements, one would expect T_b to be well above ambient temperature for all these frequencies.

Only larger values of K_{eff} would explain the measured radio-frequency losses at 297 K. Contrapositively, to minimize losses at radio frequencies, as represented by the imaginary part of susceptibility, small particles with small K_{eff} will yield high Néel relaxation frequencies and, equivalently, low blocking temperatures.

3) ANISOTROPY FROM QUASI-STATIC BLOCKING TEMPERATURE

The blocking temperature T_b below which magnetic viscosity appears is a function of the measurement field H in addition to the measurement frequency. As summarized by Knobel et al. [84],

$$T_b = \frac{K_{eff}V}{k\ln\left[(1/f)/\tau_0\right]}\left[1-\left(\frac{H}{H_a}\right)\right]^{3/2}, \tag{45}$$

where the uniaxial anisotropy field is [81], [92]

$$H_a = \frac{2K_{eff}}{\mu_0 M_s}. \tag{46}$$

Of course, Eq. (45) breaks down for $H > H_a$. The denominator of Eq. (45) is relatively insensitive to the values of $1/f$ and τ_0 for low-frequency measurements. Other field-dependence formulations are reviewed by El-Hilo et al. [89]. (The measurements depicted in Figs. 6–23 are practically in zero field.)

The effective anisotropy constant K_{eff} may be estimated numerically from Eq. (45) and measurements of T_b, which

[23] In Rosensweig's book [88], $\tau_N \approx 0.1$ μs for 10 nm particles, which would imply $K_{eff} \approx 36$ kJ/m^3.

is often associated with a peak in zero-field-cooled magnetization as a function of temperature. In Fig. 5, for frozen PBG 200 and a measurement field H of 800 A/m, such a peak is tenuous. However, the bifurcation of the zero-field-cooled and field-cooled curves at 238 K, associated with the blocking of the largest particles, is well defined. For the present demonstration, it will suffice to define a T_b of 238 K for particles of diameter 13 nm, the largest particles as modeled in Fig. 4.

For 13 nm particles, $M_s = 328$ kA/m (independent of particle size), $H = 800$ A/m, $1/f = 12$ s (the time for a temperature increase of 1 K before each measurement point, itself another approximation), $\tau_0 = 0.1$ ns, and $T_b = 238$ K, one obtains $K_{eff} = 73$ kJ/m^3. Such large values of K_{eff} have been noted occasionally [82] and may be attributed to particle interactions [49], [93], [94], or particle defects such as antiphase boundaries [57].

If one used $K_{eff} = 73$ kJ/m^3 to predict the lossy high-frequency response of 9.5 nm particles at 297 K in near-zero field, with $\tau_0 = 0.1$ ns, one would obtain $\tau_N = 295$ ns, equivalent to a not unreasonable Néel relaxation frequency $1/\tau_N = 3.4$ MHz, Eq. (42). From Eq. (44), one could calculate values of $T_b = 258$ K for measurements at $f = 1$ MHz, $T_b = 344$ K at $f = 10$ MHz, $T_b = 515$ K at $f = 100$ MHz, and $T_b = 1031$ K at $f = 1$ GHz (summarized in Table 3).

Normally, the expected susceptibility for truly blocked particles would be zero. However, if particles actually had uniaxial anisotropy, as assumed in Eq. (45), small but measurable susceptibilities would be obtained according to the Stoner-Wohlfarth model: The susceptibility of spatially averaged blocked particles would be $\chi = \mu_0 M_s^2/3K_{eff}$, as demonstrated by Iglesias et al. [95] and Zambach et al. [14]. For $M_s = 328$ kA/m and $K_{eff} = 73$ kJ/m^3, one would obtain $\chi = 0.6$; for $K_{eff} = 36$ kJ/m^3, $\chi = 1.3$.

C. PARTICLE SIZE EFFECTS

For the particles' magnetic moments to respond without loss to an alternating field, f must be smaller than $1/\tau_N$. When f is many orders of magnitude larger than $1/\tau_N$, the particles are blocked.

In addition to the relative magnitudes of the measurement frequency f and the blocking frequency $1/\tau_N$, the relative magnitudes of $K_{eff}V$ and k_BT are important. When $K_{eff}V < kT$, the exponential in the Néel relaxation equation is on the order of unity, so τ_N is determined by the value of τ_0 and is insensitive to moderate changes in particle size or particle size distributions. This was evident above, when only magnetocrystalline anisotropy was considered.

This is quite different from the dramatic effect of particle size on τ_N for materials with $K_{eff}V > kT$ described by Bean and Livingston [2] and recounted in many textbooks: For iron particles with ⟨100⟩ easy axes, $K_1 = 48$ kJ/m^3 [81], [92] and $K_{eff}V = K_1V/4$ [2], [7]. In the classic example of blocked 30 nm iron particles at ambient temperature, $K_{eff}V/kT \approx 41$ (i.e., $K_{eff}V \gg kT$), so $\exp\left(K_{eff}V/kT\right) \approx 9 \times 10^{17}$, and with the assumption $\tau_0 = 1$ ns, $\tau_N \approx 10^9$ s, seven orders of magnitude larger than the measurement time $1/f = 100$ s [2]. For unblocked 23 nm iron particles, $K_{eff}V/kT \approx 19$, so $\exp\left(K_{eff}V/kT\right) \approx 2 \times 10^8$, still large, but $\tau_N \approx 0.1$ s, three orders of magnitude smaller than $1/f = 100$ s.

The 9.5 nm magnetite particles measured here are magnetically viscous but not blocked in the 1 MHz – 1 GHz frequency range of the susceptibility measurements. If one took τ_N to be as small as 1 μs, it would be only three orders of magnitude larger than the smallest measurement time $1/f = 1$ ns, not close to the seven orders of magnitude larger that is seemingly required for hard blocking.

The notable decrease in permeability and susceptibility up to about $f = 200$ MHz ($1/f = 5$ ns) seen in the figures, independent of any Brownian relaxation effects at these frequencies, may be readily explained by the blocking of the larger particles in the size distribution with increasing frequency. As in the case of 30 nm iron particles described above, one may use, as the criterion for hard blocking, τ_N exceeding $1/f$ by seven orders of magnitude or more ($f \lll 1/\tau_N$). For example, from Eq. (42), at 297 K, with $\tau_0 = 0.1$ ns and $K_{eff} = 73$ kJ/m^3 (Table 3), one obtains $\tau_N \geq 50$ ms for particles of diameter 13 nm and larger. Such τ_N exceed $1/f = 5$ ns by at least seven orders of magnitude. If instead one used $\tau_0 = 1$ ns and $K_{eff} = 67$ kJ/m^3, one would obtain $\tau_N \geq 50$ ms for particles of diameter 12.8 nm and larger.

It is entirely evident, even if one assumes the veracity of Eq. (42), that uncertainty in both τ_0 and K_{eff} undermines an accurate estimation of τ_N. Instead, one may be guided by the presence of losses at a given measurement frequency to postulate the value of $1/\tau_N$ to be a lower frequency.

D. FERROMAGNETIC RESONANCE

A third dynamic mechanism is ferromagnetic resonance (FMR), specifically zero-field FMR. The Larmor FMR frequency is

$$f_L = \frac{\mu_0 H_a \gamma_m}{2\pi}, \tag{47}$$

where $\gamma_m/2\pi$ is the gyromagnetic ratio, μ_0 is the permeability of vacuum, and H_a is an anisotropy field. The Landé g-factor for magnetite [96] is 2.12 (compared to 2.002 for free electrons), which gives $\gamma_m/2\pi = 2.97 \times 10^{10}$ Hz/T.

If just magnetocrystalline anisotropy were considered, then H_a is the magnetocrystalline anisotropy field,

$$H_a = -\frac{4K_1}{3\mu_0 M_s}, \tag{48}$$

where M_s is the saturation magnetization [81], [92]. Again, K_2 is ignored. For $M_s = 328$ kA/m (from Section III-C above) and $K_1 = -11$ kJ/m^3, $H_a = 35.6$ kA/m and $f_L = 1.3$ GHz.

For a larger effective anisotropy constant, $K_{eff} \approx 73$ kJ/m^3, one would consider an overall uniaxial anisotropy, Eq. (46), $H_a = 2K_{eff}/\mu_0 M_s = 354$ kA/m and calculate a Larmor precession frequency $f_L = 13$ GHz.

For relatively large K_{eff}, the calculated Néel relaxation frequency is 0.7 MHz $\lesssim 1/\tau_N \lesssim$ 3.4 MHz (Table 3). It is reasonable to believe that $1/\tau_N < 1$ MHz for these nanoparticles at

TABLE 3. For 9.5 nm magnetite particles at $T = 297$ K, calculated values of Néel relaxation frequency $1/\tau_N$, from Eq. (42), and blocking temperatures T_b at frequencies f of 1 MHz, 10 MHz, and 100 MHz from Eq. (44), for different ranges of effective anisotropy K_{eff} and for two possible energy-barrier attempt times τ_0. The relatively low magnetocrystalline anisotropy energy $K_{eff}V$ compared to thermal energy kT (i.e., $K_{eff}V/kT < 1$) would imply simple superparamagnetic (SPM) behavior with no magnetic viscosity at ambient temperature, which is not the case for these ferrofluids. Larger $K_{eff}V$ is consistent with magnetic viscosity at radio frequencies. Similarly, measurement frequency f (for example, 100 MHz) compared to $1/\tau_N$ defines the regimes $f \ll 1/\tau_N$, $f \sim 1/\tau_N$, and $f > 1/\tau_N$. For $f \gg 1/\tau_N$, the particles would be blocked.

Anisotropy	K_{eff} (kJ/m³)	τ_0 (ns)	$1/\tau_N$ (MHz)	T_b (K) at 1 MHz	T_b (K) at 10 MHz	T_b (K) at 100 MHz	$K_{eff}V/kT$	f (= 100 MHz)	Expected Behavior
Magneto-crystalline	0.9	0.1	9062	3	4	6	0.1	$f \ll 1/\tau_N$	SPM
		1	906	4	6	13			
Larger anisotropies	36	0.1	194	127	170	254	3.9	$f \sim 1/\tau_N$	Viscous
		1	19	170	254	508			
From quasi-static T_b	73	0.1	3.4	258	344	515	8	$f > 1/\tau_N$	Viscous
	67	1	0.7	237	315	473	7		

ambient temperature, which would explain the susceptibility having both real and imaginary parts over the 1 MHz – 1 GHz frequency range. As f_L is approached at higher frequencies, the imaginary susceptibility would increase.

For applications that require magnetic nanoparticles with high susceptibility and low loss at radio frequencies, such as on-chip voltage converters, an attempt could be made to optimize both FMR frequency f_L and blocking frequency $1/\tau_N$ so that they are above the intended operation frequencies. Materials with large K_{eff} or small M_s would satisfy the f_L requirement, although the latter would reduce susceptibility. High $1/\tau_N$ could be achieved with small K_{eff} or small particle volumes. Strategies along these lines are described by Hasegawa et al. [97] and Song et al. [55]. Larger, multidomain ferromagnetic particles would have different considerations.

V. EPILOGUE

Superparamagnetic blocking is a function of temperature, field, and frequency. At ambient temperature, very small fields, and radio frequencies, the studied superparamagnetic particles are magnetically viscous and hysteretic, with $\chi_0' > 0$ and $\chi_0'' > 0$, but not blocked, which would be characterized by zero susceptibility or, in the case of uniaxial anisotropy, very small susceptibility. Low-field magnetic viscosity occurs over an extended range of radio frequencies at ambient temperature, above the blocking temperature as it is traditionally measured using quasi-static magnetometry.

One might ponder if it is legitimate to apply superparamagnetic theory to the behavior of nanoparticles in their viscous state at radio frequencies. The question revolves around whether Langevin theory, which is extensible from paramagnetism to superparamagnetic particles, can be further extended to viscous superparamagnetic particles. If one considered the absolute value of complex susceptibility as representing the response to an alternating field, Langevin theory should indeed apply. Application to the complex components of susceptibility is a natural extension.

A relaxation model for superparamagnetic particles at radio frequencies, which remains to be fully tested for monodisperse particles, is this:

$$f \ll \frac{1}{\tau_N} \text{ (thermodynamic equilibrium, lossless)}$$

$$f > \frac{1}{\tau_N} \begin{cases} K_{eff}V < kT \text{ (thermodynamic equilibrium, lossless)} \\ K_{eff}V > kT \text{ (magnetic viscosity, losses)} \\ K_{eff}V \gg kT \text{ (blocked)} \end{cases}$$

$$f \ggg \frac{1}{\tau_N} \text{ (blocked)}$$

The imaginary (absorptive, resistive, loss) part of susceptibility increases with frequency above the Néel relaxation frequency $1/\tau_N$ as ferromagnetic resonance is approached. The range 1 MHz – 1 GHz is in the magnetic viscosity range for superparamagnetism and above $1/\tau_N$ for 9.5 nm magnetite particles at ambient temperature.

Fannin [74] addresses frequency-dependent complex susceptibility in the context of Langevin paramagnetism. Support for a dynamic Langevin theory of superparamagnetism is found in an article by Barrera et al. [98], which derives analytic expressions for magnetization harmonics at kilohertz frequencies. Their analysis is for $K_{eff}V > kT$.

Regarding the interaction models, the complex modified mean-field model, although it is computationally the most cumbersome, is a nice middle-ground between the Onsager model, which provides an upper bound, and the Weiss molecular-field model, which depends on the choice of molecular field constant γ, but generally serves as a lower bound. As interactions decrease, exemplified by more dilute solutions, the Onsager model and the Weiss model converge to the modified mean-field model.

Once the intrinsic susceptibility is obtained, susceptibilities for solutions and composites of arbitrary concentrations can be predicted according to the traditional approach, in which the intrinsic Langevin susceptibility is assumed. However, the traditional approach does not consider complex or frequency-dependent susceptibilities.

Here is a summary of the main points of the article: (1) Single-domain magnetic particles have important applications at radio frequencies, where they are magnetically

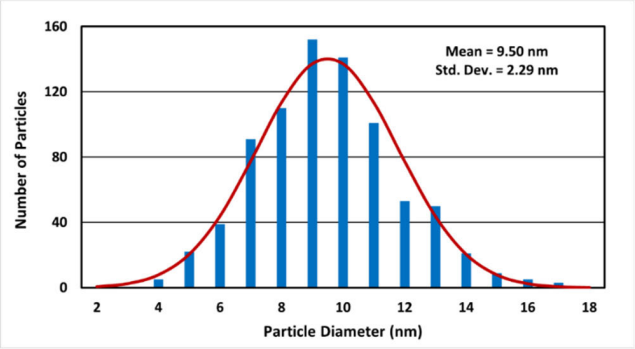

FIGURE 24. Distribution of particle diameters provided by the manufacturer with an amplitude fit to a normal distribution based on the sample mean and standard deviation.

viscous. (2) Susceptibility measurements of toroids eliminate the need to consider demagnetizing factors of composites of single-domain particles. (3) The effect of dipolar interactions among superparamagnetic particles can be removed using established interaction models to obtain the intrinsic susceptibility of noninteracting particles. (4) Some interaction models implicitly assume overall interparticle interactions that support alignment with an applied field. (5) For particles on the order of 10 nm in diameter at ambient temperature, the Langevin analysis for superparamagnetism can be extended to radio frequencies, where susceptibility is a complex quantity. (6) Magnetic figures of merit for magnetically viscous nanoparticle composites are the real and imaginary parts of susceptibility normalized by the composite filling fraction. The latter is a better metric for losses compared to the traditional loss tangent. (7) Because calculations of Néel relaxation times τ_N are only estimates owing to uncertainties in both τ_0 and K_{eff}, it is best to be guided by experimental indications of viscosity and blocking. At radio frequencies, the blocking temperature T_b for these ferrofluids is above ambient temperature. (8) The concept of blocking frequency is as relevant as that of blocking temperature. (9) Magnetic viscosity covers many orders of magnitude in time. Hard blocking requires $K_{eff}V \gg kT$ or $f \ggg 1/\tau_N$. (10) It should be possible to optimize nanoparticle size and anisotropy for low-loss applications at radio frequencies.

APPENDIXES

A. MEAN SPHERICAL PARTICLE DIAMETER

A mean particle diameter of 9.50 nm and a standard deviation of 2.29 nm were obtained by direct calculation of the mean and standard deviation of the particle diameter distribution provided by the ferrofluid manufacturer (Fig. 24). A normal distribution with those values of mean and standard deviation is also displayed. One can only weakly claim that the diameters are normally distributed because the sample size is small, the measurements are binned, and the measurement uncertainty is unknown.

Alternative approaches to determine average particle diameter and standard deviation include fitting to normal and log-normal distributions. A typical fitting criterion is minimization of the square of the differences between the actual and expected number of occurrences. One might prefer to minimize the chi-squared statistic, which gives similar results but allows a direct test of goodness of fit. Such a Gaussian fit with a chi-squared criterion yields a mean of 9.46 nm and a standard deviation of 2.33 nm. (The three determinations of 17 nm were excluded from both the fit and a chi-squared goodness-of-fit analysis because they are fewer than the usual minimum of five.) For 10 degrees of freedom (13 diameter categories minus the 2 estimates of mean and standard deviation minus 1), a chi-squared of 18.2 of the fit corresponds to a p-value of 0.052, which is greater than the usual 0.050 criterion. Thus, one cannot reject the null hypothesis that the data are drawn from a normal population.

Log-normal distributions often characterize particle diameters [19], [86], [99], [100]. If particle diameters are logarithmically distributed, so are particle volumes. For the particle diameter distribution here, the goodness of a log-normal fit is notably worse than that of the simple normal fit. The mean and standard deviation of the logarithms of the diameters that are fit to a normal distribution (with an unconstrained total number concentration) are 2.16 and 0.26, which, when exponentiated, give a median diameter of 8.64 nm (corresponding to a geometric mean of equal value), a standard deviation of 2.41 nm, and an arithmetic mean of 8.95 nm.

B. MAGNETIC POLARIZABILITY

Although it is not often used in magnetics, one can define an isotropic magnetic dipolar orientational polarizability per particle (or simply "magnetic polarizability," not to be confused with magnetic polarization),[24]

$$\beta = \frac{\mu_0 m^2}{3k_B T}. \tag{A1}$$

This is the classic Langevin-Debye equation [64], [102], [103]. Debye applied Langevin's orientation-averaging formulation for the mean magnetic moment of gas molecules carrying a permanent magnetic moment to electrically polar molecules. Here, Debye's formulation of electric polarizability is applied to superparamagnetic particles.

Magnetic polarizability is more generally defined as

$$\beta = \frac{\langle m \rangle}{H}, \tag{A2}$$

where $\langle m \rangle$ is the average moment per particle in the field direction. In Eq. (7), $M = \langle m \rangle N/V = \langle m \rangle n$. Therefore, β is closely related to χ_0. From the Langevin equation for χ_0, Eq. (9),

$$\beta = \frac{\chi_0}{n} = \frac{\chi_0 V_{1p}}{\phi}. \tag{A3}$$

[24]The symbol α (different from Eq. (8)'s α) is used universally for electric polarizability. The use of β for magnetic polarizability, as by Taylor [101] for example, is less established.

Although it is normally a symmetric tensor, β is a scalar for isotropic materials. The units for β are [m^3] or, more convenient for nanoparticles, [nm^3].

If χ_0 is a complex quantity, so is β. As a figure of merit, β is superior to χ_0 because it is normalized to the number of particles that give rise to the particles' individual (not average) magnetic moment m. However, β is inferior to χ_0/ϕ because it depends on V_{1p} and because the quantity, magnetic polarizability, is unfamiliar to most magnetics practitioners.

C. PERMEABILITY OF "PARAMAGNETIC" WATER

In the frequency range from 450 MHz to 1 GHz, an apparent ''paramagnetic'' permeability of water cannot be ignored for dilute solutions. Therefore, the shorted magnetic material test fixture used with the impedance analyzer should be compensated with a capsule containing approximately the same volume of water as the colloidal solution under test.

Water, of course, is diamagnetic. However, as measured by Gutiérrez-Mejía and Ruiz-Suárez [104], it appeared to be weakly paramagnetic between 500 kHz and their maximum frequency of 1 MHz. This anomalous behavior is even more pronounced at higher frequencies (Fig. 25). It is due to the effect of the permittivity (not permeability) of water on inductance measurements and the fact that the coil measurements of Gutiérrez-Mejía and Ruiz-Suárez and the impedance analyzer method here are both based on measurements of inductance.

As explained by Payne [105], a coil's inductance naturally increases with frequency as the self-resonant frequency is approached. A dielectric in the coil reduces its resonant frequency, so the increase in inductance becomes apparent at lower frequencies. The dielectric constant of water at ambient temperature is relatively large, about 78 [106], so its effect is measurable in the megahertz range.

Similar principles apply to inductance measurements using an impedance analyzer and a shorted coaxial transmission line. As pointed out in an application note [107], ''When measuring a magnetic material with a high [relative] permittivity (near 10 or above), precise measurements cannot be performed near 1 GHz. Permeability is derived from the inductance value of the combined impedance of the MUT [material under test] and the fixture. The measured impedance should [have] a negligible amount of capacitance. When the magnetic material's permittivity is high, current flows through the space between the MUT and the fixture. This is equivalent to a capacitor connected in parallel to . . . the MUT. This parallel *LC* circuit causes an impedance-resonance at a [lower] frequency. The higher the permittivity, the lower the resonant frequency will be . . . .''

Whereas water has a relative permittivity of about 78, that of ice is much lower, about 3 [108]. This does not reduce the resonant frequency very much, so the measured permeability remains closer to unity at high frequencies and below unity at frequencies below 450 MHz. This is consistent with the low-frequency coil measurements of ice by Gutiérrez-Mejía and Ruiz-Suárez.

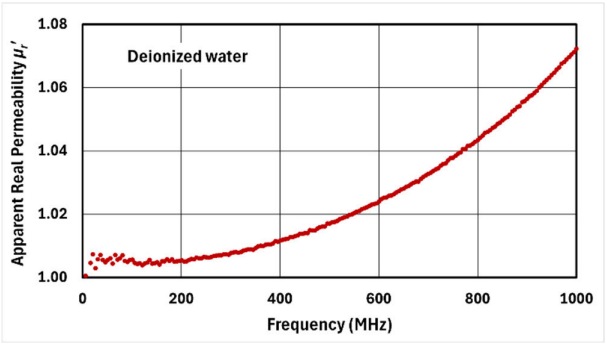

FIGURE 25. Apparent real part of relative permeability of a toroid of deionized water. The high permittivity of water causes it to appear to be paramagnetic at high frequencies. The imaginary part of permeability (not shown) is zero within experimental error at all frequencies.

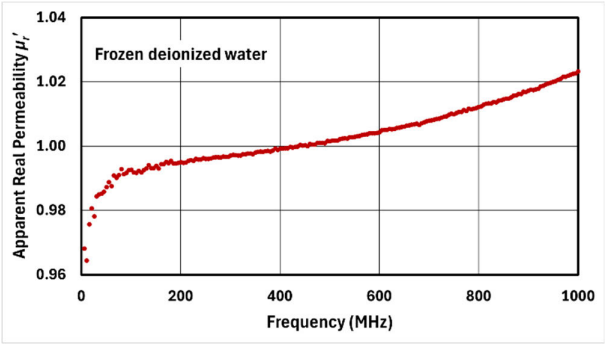

FIGURE 26. Apparent real part of relative permeability of a toroid of frozen deionized water. The relatively low permittivity of ice reduces its effect on the permeability measurement. The imaginary part of permeability (not shown) is zero within experimental error at all frequencies.

ACKNOWLEDGMENT

Dialogue with colleagues contributed to the development of this article: Samuel D. Oberdick and Montserrat Rivas (demagnetizing factors of superparamagnetic composites), Alexey V. Nazarov (magnetometer measurements), Margo Hauwaert and James C. Booth (radio-frequency measurements), Pavel Kabos (ferromagnetic resonance measurements), Anthony B. Kos (switching converters), and R. G. Don Grainger, Michael R. Frey, and Bradley K. Alpert (particle size distributions). Anthony B. Kos and Stephen E. Russek helped with data acquisition and sample holders for preliminary measurements made using Hewlett-Packard 4191A and 4194A impedance analyzers. Samuel D. Oberdick, Sara A. Majetich, Mathias Zambach, Jonathan Leliaert, and Marco Beleggia offered valuable comments and suggestions on the manuscript.

A symbolic manipulation program, Mathematica 13.2, was used to verify some of the equations of complex variables. No generative artificial-intelligence large language model was used in writing this article. Certain instruments, materials, and software applications are identified in order to specify the experimental procedure adequately. This is not intended

to imply recommendation or endorsement of any product by NIST, nor is it intended to imply that the items identified are necessarily the best available for the purpose. The data for this article are available in the NIST Public Data Repository, https://doi.org/10.18434/mds2-3991, published 25 September 2025.

REFERENCES

[1] C. P. Bean, "Hysteresis loops of mixtures of ferromagnetic micropowders," *J. Appl. Phys.*, vol. 26, no. 11, pp. 1381–1383, Nov. 1955, doi: 10.1063/1.1721912.

[2] C. P. Bean and J. D. Livingston, "Superparamagnetism," *J. Appl. Phys.*, vol. 30, no. 4, pp. S120–S129, Apr. 1959, doi: 10.1063/1.2185850.

[3] W. Wernsdorfer, E. Bonet Orozco, K. Hasselbach, A. Benoit, B. Barbara, N. Demoncy, A. Loiseau, H. Pascard, and D. Mailly, "Experimental evidence of the Néel–Brown model of magnetization reversal," *Phys. Rev. Lett.*, vol. 78, no. 9, pp. 1791–1794, Mar. 1997, doi: 10.1103/PhysRevLett.78.1791.

[4] E. Tirosh, B. Tsukerman, N. Taub, S. A. Majetich, and G. Markovich, "Magnetoresistive telegraph noise in Langmuir–Blodgett films of colloidal magnetite nanocrystals as seen via scanning tunneling microscopy," *Phys. Rev. B, Condens. Matter*, vol. 80, no. 22, Dec. 2009, Art. no. 224427, doi: 10.1103/physrevb.80.224427.

[5] S. K. Piotrowski, M. F. Matty, and S. A. Majetich, "Magnetic fluctuations in individual superparamagnetic particles," *IEEE Trans. Magn.*, vol. 50, no. 11, Nov. 2014, Art. no. 2303704, doi: 10.1109/TMAG.2014.2321327.

[6] O. Sinwani, J. W. Reiner, and L. Klein, "Monitoring superparamagnetic Langevin behavior of individual $SrRuO_3$ nanostructures," *Phys. Rev. B*, vol. 89, no. 2, Jan. 2014, Art. no. 020404, doi: 10.1103/physrevb.89.020404.

[7] C. J. Lin, "Behavior of ferro- or ferrimagnetic very fine particles," *J. Appl. Phys.*, vol. 32, no. 3, pp. S233–S234, Mar. 1961, doi: 10.1063/1.2000415.

[8] C. P. Bean and I. S. Jacobs, "Magnetic granulometry and superparamagnetism," *J. Appl. Phys.*, vol. 27, no. 12, pp. 1448–1452, Dec. 1956, doi: 10.1063/1.1722287.

[9] C. G. Montgomery, "The magnetization of colloidal suspensions," *Phys. Rev.*, vol. 38, no. 9, p. 1782, Nov. 1931, doi: 10.1103/physrev.38.1782.

[10] W. C. Elmore, "The magnetization of ferromagnetic colloids," *Phys. Rev.*, vol. 54, no. 12, pp. 1092–1095, Dec. 1938, doi: 10.1103/physrev.54.1092.

[11] H. B. G. Casimir, *Magnetism and Very Low Temperatures*. Cambridge, U.K.: Cambridge Univ. Press, 1940, p. 11, pp. 56–60.

[12] R. Skomski, G. C. Hadjipanayis, and D. J. Sellmyer, "Effective demagnetizing factors of complicated particle mixtures," *IEEE Trans. Magn.*, vol. 43, no. 6, pp. 2956–2958, Jun. 2007, doi: 10.1109/TMAG.2007.893798.

[13] B. Bleaney and R. A. Hull, "The effective susceptibility of a paramagnetic powder," *Proc. Roy. Soc. London*, vol. 178, no. 972, pp. 86–92, May 1941, doi: 10.1098/rspa.1941.0045.

[14] M. Zambach, Z. Ouyang, M. Knaapila, M. Beleggia, and C. Frandsen, "Design of superparamagnetic nanoparticle-materials for high-frequency inductor cores," *APL Mater.*, vol. 13, no. 7, Jul. 2025, Art. no. 071128, doi: 10.1063/5.0275285.

[15] M. Zambach, M. Varón, M. R. Almind, M. Knaapila, Z. Ouyang, M. Beleggia, and C. Frandsen, "Demagnetisation effects in single-domain particles," 2025, *arXiv:2502.03394*.

[16] K. M. Chowdary and S. A. Majetich, "Frequency-dependent magnetic permeability of $Fe_{10}Co_{90}$ nanocomposites," *J. Phys. D, Appl. Phys.*, vol. 47, no. 17, Apr. 2014, Art. no. 175001, doi: 10.1088/0022-3727/47/17/175001.

[17] J. J. Becker, "Magnetic method for the measurement of precipitate particle sizes in a Cu-Co alloy," *JOM*, vol. 9, no. 1, pp. 59–63, Jan. 1957, doi: 10.1007/bf03398452.

[18] J. W. Cahn, "Discussion of magnetic method for the measurement of precipitate particle sizes in a Cu-Co alloy," *JOM*, vol. 9, no. 10, p. 1309, Oct. 1957, doi: 10.1007/BF03398313.

[19] R. Chantrell, J. Popplewell, and S. Charles, "Measurements of particle size distribution parameters in ferrofluids," *IEEE Trans. Magn.*, vol. TM-14, no. 5, pp. 975–977, Sep. 1978, doi: 10.1109/TMAG.1978.1059918.

[20] A. Jillavenkatesa, S. J. Dapkunas, and L.-S. H. Lum, "Particle size characterization," Nat. Inst. Stand. Tech., Washington, DC, USA, Sp. Pub. 960-1, Jan. 2001. [Online]. Available: https://nvlpubs.nist.gov/nistpubs/Legacy/SP/nistspecialpublication960-1.pdf

[21] A. O. Ivanov, S. S. Kantorovich, E. N. Reznikov, C. Holm, A. F. Pshenichnikov, A. V. Lebedev, A. Chremos, and P. J. Camp, "Magnetic properties of polydisperse ferrofluids: A critical comparison between experiment, theory, and computer simulation," *Phys. Rev. E, Stat. Phys. Plasmas Fluids Relat. Interdiscip. Top.*, vol. 75, no. 6, Jun. 2007, Art. no. 061405, doi: 10.1103/physreve.75.061405.

[22] I. Rehberg, R. Richter, S. Hartung, N. Lucht, B. Hankiewicz, and T. Friedrich, "Measuring magnetic moments of polydisperse ferrofluids utilizing the inverse Langevin function," *Phys. Rev. B, Condens. Matter*, vol. 100, no. 13, Oct. 2019, Art. no. 134425, doi: 10.1103/physrevb.100.134425.

[23] P. Langevin, "Sur la théorie du magnétisme," *J. Physique Theor. Appl.*, vol. 4, no. 1, pp. 678–693, 1905, doi: 10.1051/jphystap:019050040067800.

[24] P. Weiss, "L'hypothèse du champ moléculaire et la propriété ferromagnétique," *J. Physique Theor. Appl.*, vol. 6, no. 1, pp. 661–690, 1907, doi: 10.1051/jphystap:019070060066100.

[25] P. Weiss, "The magnetic properties of the alloys of the ferromagnetic metals: Iron-nickel, nickel-cobalt, cobalt-iron," *Trans. Faraday Soc.*, vol. 8, pp. 149–156, Oct. 1912, doi: 10.1039/tf9120800149.

[26] H. A. Lorentz, *The Theory of Electrons and Its Applications to the Phenomena of Light and Radiant Heat*, 2nd ed., Leipzig, Germany: B. G. Teubner, 1916, pp. 137–139, pp. 305–308. [Online]. Available: https://books.google.com/books?hl=en&lr=&id=ymBDAAAAIAAJ

[27] R. B. Goldfarb and C. E. Patton, "Superparamagnetism and spin-glass freezing in nickel-manganese alloys," *Phys. Rev. B, Condens. Matter*, vol. 24, no. 3, pp. 1360–1373, Aug. 1981, doi: 10.1103/physrevb.24.1360.

[28] K. O'Grady, A. Bradbury, S. W. Charles, S. Menear, J. Popplewell, and R. W. Chantrell, "Curie–Weiss behavior in ferrofluids," *J. Magn. Magn. Mater.*, vols. 31–34, pt. 2, pp. 958–960, Feb. 1983, doi: 10.1016/0304-8853(83)90755-2.

[29] A. F. Pshenichnikov, "Equilibrium magnetization of concentrated ferrocolloids," *J. Magn. Magn. Mater.*, vol. 145, no. 3, pp. 319–326, Mar. 1995, doi: 10.1016/0304-8853(94)01632-1.

[30] F. Söffge and E. Schmidbauer, "AC susceptability and static magnetic properties of an Fe_3O_4 ferrofluid," *J. Magn. Magn. Mater.*, vol. 24, no. 1, pp. 54–66, Jul. 1981, doi: 10.1016/0304-8853(81)90100-1.

[31] J. Popplewell, B. Abu Aisheh, and N. Y. Ayoub, "The effect of particle interactions on Curie–Weiss behavior in ferrofluids," *J. Appl. Phys.*, vol. 64, no. 10, pp. 5852–5854, Nov. 1988, doi: 10.1063/1.342203.

[32] M. El-Hilo, K. O'Grady, and R. W. Chantrell, "The ordering temperature in fine particle systems," *J. Magn. Magn. Mater.*, vol. 117, nos. 1–2, pp. 21–28, Nov. 1992, doi: 10.1016/0304-8853(92)90286-w.

[33] M. Hanson, C. Johansson, M. S. Pedersen, and S. Mørup, "The influence of particle size and interactions on the magnetization and susceptibility of nanometre-size particles," *J. Phys., Condens. Matter*, vol. 7, no. 48, pp. 9269–9277, Nov. 1995, doi: 10.1088/0953-8984/7/48/016.

[34] L. Onsager, "Electric moments of molecules in liquids," *J. Amer. Chem. Soc.*, vol. 58, no. 8, pp. 1486–1493, Aug. 1936, doi: 10.1021/ja01299a050.

[35] F. C. Frank, "A comparison of Debye's and Onsager's theories of the dielectric constants of concentrated polar media," *Trans. Faraday Soc.*, vol. 42, pp. A019–A024, Jan. 1946, doi: 10.1039/tf946420a019.

[36] J. L. Dormann, D. Fiorani, and E. Tronc, "Magnetic relaxation in fine-particle systems," *Adv. Chem. Phys.*, vol. 98, pp. 283–494, Jun. 1997, doi: 10.1002/9780470141571.ch4.

[37] A. F. Pshenichnikov, V. V. Mekhonoshin, and A. V. Lebedev, "Magneto-granulometric analysis of concentrated ferrocolloids," *J. Magn. Magn. Mater.*, vol. 161, pp. 94–102, Aug. 1996, doi: 10.1016/s0304-8853(96)00067-4.

[38] A. V. Lebedev, V. I. Stepanov, A. Kuznetsov, A. O. Ivanov, and A. F. Pshenichnikov, "Dynamic susceptibility of a concentrated ferrofluid: The role of interparticle interactions," *Phys. Rev. E, Stat. Phys. Plasmas Fluids Relat. Interdiscip. Top.*, vol. 100, no. 3, Sep. 2019, Art. no. 032605, doi: 10.1103/physreve.100.032605.

[39] X. Batlle, N. Pérez, P. Guardia, O. Iglesias, A. Labarta, F. Bartolomé, L. M. García, J. Bartolomé, A. G. Roca, M. P. Morales, and C. J. Serna, "Magnetic nanoparticles with bulklike properties," *J. Appl. Phys.*, vol. 109, no. 7, Apr. 2011, Art. no. 07B524, doi: 10.1063/1.3559504.

[40] E. Wetterskog, M. Agthe, A. Mayence, J. Grins, D. Wang, S. Rana, A. Ahniyaz, G. Salazar-Alvarez, and L. Bergström, "Precise control over shape and size of iron oxide nanocrystals suitable for assembly into ordered particle arrays," *Sci. Technol. Adv. Mater.*, vol. 15, no. 5, Oct. 2014, Art. no. 055010, doi: 10.1088/1468-6996/15/5/055010.
[41] R. B. Goldfarb and H. E. Bussey, "Method for measuring complex permeability at radio frequencies," *Rev. Sci. Instrum.*, vol. 58, no. 4, pp. 624–627, Apr. 1987, doi: 10.1063/1.1139227.
[42] Hewlett-Packard Co., *HP Test & Measurement Catalog 1997*, Palo Alto, CA, USA, 1996, p. 352. [Online]. Available: http://hparchive.com/Catalogs/HP-Catalog-1997.pdf
[43] Hewlett-Packard Co., "Solutions for measuring permittivity and permeability," Appl. Note 1297, 1997. [Online]. Available: https://www.hpmemoryproject.org/an/pdf/an_1297.pdf
[44] J. Baker-Jarvis, M. D. Janezic, J. H. Grosvenor, and R. G. Geyer, "Transmission/reflection and short-circuit line methods for measuring permittivity and permeability," Nat. Inst. Stand. Technol., Washington, DC, USA, Tech. Note 1355-R, Dec. 1993. [Online]. Available: https://archive.org/details/transmissionrefl1355bake_0
[45] V. K. Sakharov, R. A. Booth, and S. A. Majetich, "High-frequency permeability of Ni and Co particle assemblies," *J. Appl. Phys.*, vol. 115, no. 17, Feb. 2014, Art. no. 17A517, doi: 10.1063/1.4866234.
[46] S. Takeda, T. Hotchi, S. Motomura, and H. Suzuki, "Theoretical consideration on short- & open-circuited transmission lines for permeability & permittivity measurement," *J. Magn. Soc. Jpn.*, vol. 39, no. 3, pp. 116–120, 2015, doi: 10.3379/msjmag.1504r006.
[47] D.-X. Chen, J. A. Brug, and R. B. Goldfarb, "Demagnetizing factors for cylinders," *IEEE Trans. Magn.*, vol. 27, no. 4, pp. 3601–3619, Table I, Jul. 1991, doi: 10.1109/20.102932.
[48] C. A. Domenicali, "Magnetic and electric properties of natural and synthetic single crystals of magnetite," *Phys. Rev.*, vol. 78, no. 4, pp. 458–467, May 1950, doi: 10.1103/physrev.78.458.
[49] G. F. Goya, T. S. Berquó, F. C. Fonseca, and M. P. Morales, "Static and dynamic magnetic properties of spherical magnetite nanoparticles," *J. Appl. Phys.*, vol. 94, no. 5, pp. 3520–3528, Sep. 2003, doi: 10.1063/1.1599959.
[50] S. J. Kemp, R. M. Ferguson, A. P. Khandhar, and K. M. Krishnan, "Monodisperse magnetite nanoparticles with nearly ideal saturation magnetization," *RSC Adv.*, vol. 6, no. 81, pp. 77452–77464, Aug. 2016, doi: 10.1039/c6ra12072e.
[51] Y. Hadadian, H. Masoomi, A. Dinari, C. Ryu, S. Hwang, S. Kim, B. K. Cho, J. Y. Lee, and J. Yoon, "From low to high saturation magnetization in magnetite nanoparticles: The crucial role of the molar ratios between the chemicals," *ACS Omega*, vol. 7, no. 18, pp. 15996–16012, Apr. 2022, doi: 10.1021/acsomega.2c01136.
[52] K. L. Livesey, S. Ruta, N. R. Anderson, D. Baldomir, R. W. Chantrell, and D. Serantes, "Beyond the blocking model to fit nanoparticle ZFC/FC magnetisation curves," *Sci. Rep.*, vol. 8, no. 1, Jul. 2018, Art. no. 11166, doi: 10.1038/s41598-018-29501-8.
[53] F. Fabris, K.-H. Tu, C. A. Ross, and W. C. Nunes, "Influence of dipolar interactions on the magnetic properties of superparamagnetic particle systems," *J. Appl. Phys.*, vol. 126, no. 17, Nov. 2019, Art. no. 173905, doi: 10.1063/1.5125595.
[54] J. García-Otero, M. Porto, J. Rivas, and A. Bunde, "Influence of dipolar interaction on magnetic properties of ultrafine ferromagnetic particles," *Phys. Rev. Lett.*, vol. 84, no. 1, pp. 167–170, Jan. 2000, doi: 10.1103/physrevlett.84.167.
[55] N.-N. Song, H.-T. Yang, H.-L. Liu, X. Ren, H.-F. Ding, X.-Q. Zhang, and Z.-H. Cheng, "Exceeding natural resonance frequency limit of monodisperse Fe_3O_4 nanoparticles via superparamagnetic relaxation," *Sci. Rep.*, vol. 3, no. 1, Nov. 2013, Art. no. 3161, doi: 10.1038/srep03161.
[56] C. Moya, Ó. Iglesias, X. Batlle, and A. Labarta, "Quantification of dipolar interactions in $Fe_{3-x}O_4$ nanoparticles," *J. Phys. Chem. C*, vol. 119, no. 42, pp. 24142–24148, Oct. 2015, doi: 10.1021/acs.jpcc.5b07516.
[57] Z. Nedelkoski, D. Kepaptsoglou, L. Lari, T. Wen, R. A. Booth, S. D. Oberdick, P. L. Galindo, Q. M. Ramasse, R. F. L. Evans, S. Majetich, and V. K. Lazarov, "Origin of reduced magnetization and domain formation in small magnetite nanoparticles," *Sci. Rep.*, vol. 7, no. 1, Apr. 2017, Art. no. 45997, doi: 10.1038/srep45997.
[58] S. Klomp, C. Walker, M. Christiansen, B. Newbold, D. Griner, Y. Cai, P. Minson, J. Farrer, S. Smith, B. J. Campbell, R. G. Harrison, and K. Chesnel, "Size-dependent crystalline and magnetic properties of 5–100 nm Fe_3O_4 nanoparticles: Superparamagnetism, Verwey transition, and FeO-Fe_3O_4 core-shell formation," *IEEE Trans. Magn.*, vol. 56, no. 11, Nov. 2020, Art. no. 2300109, doi: 10.1109/TMAG.2020.3018154.
[59] E. J. W. Verwey, "Electronic conduction of magnetite (Fe_3O_4) and its transition point at low temperatures," *Nature*, vol. 144, no. 3642, pp. 327–328, Aug. 1939, doi: 10.1038/144327b0.
[60] P. Weiss and R. Forrer, "La saturation absolue des ferromagnétiques et les lois d'approche en fonction du champ et de la température," *Annales de Phys.*, ser. 10, vol. 12, pp. 279–372, 1929, doi: 10.1051/anphys/192910120279.
[61] K. Renger, "Die anfängliche suszeptibilität von Eisen und Magnetit in Abhängigkeit von der Temperatur," Doctoral thesis, Dept. Tech. Sci., ETH Zürich, Zürich, Switzerland, 1913, pp. 57–60, doi: 10.3929/ethz-a-000091771.
[62] K. Abe, Y. Miyamoto, and S. Chikazumi, "Magnetocrystalline anisotropy of low temperature phase of magnetite," *J. Phys. Soc. Jpn.*, vol. 41, no. 6, pp. 1894–1902, Dec. 1976, doi: 10.1143/jpsj.41.1894.
[63] W. Huang, J. Wu, W. Guo, R. Li, and L. Cui, "Initial susceptibility and viscosity properties of low concentration ε-Fe_3N based magnetic fluid," *Nanosc. Res. Lett.*, vol. 2, no. 3, pp. 155–160, Mar. 2007, doi: 10.1007/s11671-007-9047-7.
[64] P. Debye, *Polar Molecules*. New York, NY, USA: Chemical Catalog Co., 1929, pp. 27–30, pp. 83–85, pp. 89–95. [Online]. Available: https://archive.org/details/polarmolecules0000pdeb_f1a1
[65] S. Ota and Y. Takemura, "Characterization of Néel and Brownian relaxations isolated from complex dynamics influenced by dipole interactions in magnetic nanoparticles," *J. Phys. Chem. C*, vol. 123, no. 47, pp. 28859–28866, Sep. 2019, doi: 10.1021/acs.jpcc.9b06790.
[66] S. Shtrikman and E. P. Wohlfarth, "The theory of the Vogel–Fulcher law of spin glasses," *Phys. Lett. A*, vol. 85, nos. 8–9, pp. 467–470, Oct. 1981, doi: 10.1016/0375-9601(81)90441-2.
[67] H. T. Yang, H. L. Liu, N. N. Song, H. F. Du, X. Q. Zhang, Z. H. Cheng, J. Shen, and L. F. Li, "Determination of the critical interspacing for the noninteracting magnetic nanoparticle system," *Appl. Phys. Lett.*, vol. 98, no. 15, Apr. 2011, Art. no. 153112, doi: 10.1063/1.3574917.
[68] M. Jackson and H.-U. Worm, "Anomalous unblocking temperatures, viscosity and frequency-dependent susceptibility in the chemically-remagnetized Trenton limestone," *Phys. Earth Planet Interface*, vol. 126, nos. 1–2, pp. 27–42, Oct. 2001, doi: 10.1016/s0031-9201(01)00242-4.
[69] D. Hasegawa, S. Nakasaka, M. Sato, T. Ogawa, and M. Takahashi, "Magnetization process of h.c.p.-CoIr nanoparticles with negative uniaxial magnetocrystalline anisotropy," *IEEE Trans. Magn.*, vol. 42, no. 10, pp. 2805–2807, Oct. 2006, doi: 10.1109/TMAG.2006.879886.
[70] A. S. Eggeman, S. A. Majetich, D. Farrell, and Q. A. Pankhurst, "Size and concentration effects on high frequency hysteresis of iron oxide nanoparticles," *IEEE Trans. Magn.*, vol. 43, no. 6, pp. 2451–2453, Jun. 2007, doi: 10.1109/TMAG.2007.894127.
[71] C. N. Chinnasamy, T. Ogawa, D. Hasegawa, H. T. Yang, S. D. Yoon, V. G. Harris, and M. Takahashi, "Synthesis and magnetic properties of $Co_{1-x}Ir_x$ alloy nanoparticles for high-frequency applications," *IEEE Trans. Magn.*, vol. 43, no. 6, pp. 3112–3114, Jun. 2007, doi: 10.1109/TMAG.2007.893868.
[72] T. Jonsson, P. Svedlindh, and M. F. Hansen, "Static scaling on an interacting magnetic nanoparticle system," *Phys. Rev. Lett.*, vol. 81, no. 18, pp. 3976–3979, Nov. 1998, doi: 10.1103/physrevlett.81.3976.
[73] J. L. Dormann and D. Fiorani, "Nanophase magnetic materials: Size and interaction effects on static and dynamical properties of fine particles," *J. Magn. Magn. Mater.*, vols. 140–144, pt. 1, pp. 415–418, Feb. 1995, doi: 10.1016/0304-8853(94)00591-5.
[74] P. C. Fannin, "Investigating magnetic fluids by means of complex susceptibility measurements," *J. Magn. Magn. Mater.*, vols. 258–259, pp. 446–451, Mar. 2003, doi: 10.1016/s0304-8853(02)01093-4.
[75] A. R. von Hippel, *Dielectrics and Waves*. New York, NY, USA: John Wiley, 1954, pp. 174–178. [Online]. Available: https://archive.org/details/dielectricswaves0000vonh
[76] M. I. Shliomis, A. F. Pshenichnikov, K. I. Morozov, and I. Y. Shurubor, "Magnetic properties of ferrocolloids," *J. Magn. Magn. Mater.*, vol. 85, nos. 1–3, pp. 40–46, Apr. 1990, doi: 10.1016/0304-8853(90)90013-g.
[77] P. C. Fannin and S. W. Charles, "Measurement of the Néel relaxation of magnetic particles in the frequency range 1 kHz to 160 MHz," *J. Phys. D, Appl. Phys.*, vol. 24, no. 1, pp. 76–77, Jan. 1991, doi: 10.1088/0022-3727/24/1/013.
[78] P. C. Fannin, S. W. Charles, and T. Relihan, "On the use of complex susceptibility data to complement magnetic viscosity measurements," *J. Phys. D, Appl. Phys.*, vol. 27, no. 2, pp. 189–193, Feb. 1994, doi: 10.1088/0022-3727/27/2/002.

[79] R. E. Rosensweig, "Heating magnetic fluid with alternating magnetic field," *J. Magn. Magn. Mater.*, vol. 252, pp. 370–374, Nov. 2002, doi: 10.1016/s0304-8853(02)00706-0.

[80] L. R. Bickford, J. M. Brownlow, and R. F. Penoyer, "Magnetocrystalline anisotropy in cobalt-substituted magnetite single crystals," *Proc. IEE B, Radio Electron. Eng.*, vol. 104, no. 5S, pp. 238–244, Oct. 1956, doi: 10.1049/pi-b-1.1957.0038.

[81] S. Chikazumi, *Physics of Ferromagnetism*. London, U.K.: Oxford Univ. Press, 1997, p. 251, pp. 264–265, p. 289, doi: 10.1093/oso/9780198517764.001.0001.

[82] B. H. Sohn, R. E. Cohen, and G. C. Papaefthymiou, "Magnetic properties of iron oxide nanoclusters within microdomains of block copolymers," *J. Magn. Magn. Mater.*, vol. 182, nos. 1–2, pp. 216–224, Feb. 1998, doi: 10.1016/s0304-8853(97)00675-6.

[83] R. K. Zheng, H. Gu, B. Xu, and X. X. Zhang, "The origin of the non-monotonic field dependence of the blocking temperature in magnetic nanoparticles," *J. Phys., Condens. Matter*, vol. 18, no. 26, pp. 5905–5910, Jun. 2006, doi: 10.1088/0953-8984/18/26/010.

[84] M. Knobel, W. C. Nunes, H. Winnischofer, T. C. R. Rocha, L. M. Socolovsky, C. L. Mayorga, and D. Zanchet, "Effects of magnetic interparticle coupling on the blocking temperature of ferromagnetic nanoparticle arrays," *J. Non-Crystalline Solids*, vol. 353, nos. 8–10, pp. 743–747, Apr. 2007, doi: 10.1016/j.jnoncrysol.2006.12.037.

[85] O. Petracic, "Superparamagnetic nanoparticle ensembles," *Superlattices Microstructures*, vol. 47, no. 5, pp. 569–578, May 2010, doi: 10.1016/j.spmi.2010.01.009.

[86] G. Concas, F. Congiu, G. Muscas, and D. Peddis, "Determination of blocking temperature in magnetization and Mössbauer time scale: A functional form approach," *J. Phys. Chem. C*, vol. 121, no. 30, pp. 16541–16548, Jun. 2017, doi: 10.1021/acs.jpcc.7b01748.

[87] D. A. Balaev, A. A. Krasikov, Y. V. Knyazev, S. V. Stolyar, A. O. Shokhrina, A. D. Balaev, and R. S. Iskhakov, "Interparticle magnetic interactions and the field dependence of the superparamagnetic blocking temperature in a powder system of ultrasmall nickel ferrite particles," *JETP Lett.*, vol. 120, no. 10, pp. 751–758, Nov. 2024, doi: 10.1134/s0021364024603865.

[88] R. E. Rosensweig, *Ferrohydrodynamics*. Cambridge, U.K.: Cambridge Univ. Press, 1985, p. 63. [Online]. Available: https://store.doverpublications.com/products/9780486783000

[89] M. El-Hilo, K. O'Grady, and R. W. Chantrell, "Susceptibility phenomena in a fine particle system: II. Field dependence of the peak," *J. Magn. Magn. Mater.*, vol. 114, no. 3, pp. 307–313, Aug. 1992, doi: 10.1016/0304-8853(92)90273-q.

[90] H. Li, M. T. Klem, K. B. Sebby, D. J. Singel, M. Young, T. Douglas, and Y. U. Idzerda, "Determination of anisotropy constants of protein encapsulated iron oxide nanoparticles by electron magnetic resonance," *J. Magn. Magn. Mater.*, vol. 321, no. 3, pp. 175–180, Feb. 2009, doi: 10.1016/j.jmmm.2008.08.082.

[91] D. Cabrera, T. Yoshida, T. Rincón-Domínguez, J. L. F. Cuñado, G. Salas, A. Bollero, M. P. Morales, J. Camarero, and F. J. Teran, "Superparamagnetic-blocked state transition under alternating magnetic fields: Towards determining the magnetic anisotropy in magnetic suspensions," *Nanoscale*, vol. 14, no. 24, pp. 8789–8796, May 2022, doi: 10.1039/d2nr00808d.

[92] B. D. Cullity and C. D. Graham, *Introduction to Magnetic Materials*, 2nd ed., New Jersey, NJ, USA: John Wiley, 2009, pp. 226–227, doi: 10.1002/9780470386323.

[93] M. El-Hilo, K. O'Grady, and R. W. Chantrell, "Susceptibility phenomena in a fine particle system: I. Concentration dependence of the peak," *J. Magn. Magn. Mater.*, vol. 114, no. 3, pp. 295–306, Aug. 1992, doi: 10.1016/0304-8853(92)90272-p.

[94] J. L. Dormann, L. Bessais, and D. Fiorani, "A dynamic study of small interacting particles: Superparamagnetic model and spin-glass laws," *J. Phys. C, Solid State Phys.*, vol. 21, no. 10, pp. 2015–2034, Apr. 1988, doi: 10.1088/0022-3719/21/10/019.

[95] C. A. Iglesias, J. C. R. de Araújo, E. F. Silva, M. Gamino, M. A. Correa, and F. Bohn, "Fundamental inequalities in the Stoner-Wohlfarth model," *Phys. Rev. B, Condens. Matter*, vol. 106, no. 9, Sep. 2022, Art. no. 094405, doi: 10.1103/physrevb.106.094405.

[96] L. R. Bickford, "Ferromagnetic resonance absorption in magnetite single crystals," *Phys. Rev.*, vol. 78, no. 4, pp. 449–457, May 1950, doi: 10.1103/physrev.78.449.

[97] D. Hasegawa, H. Yang, T. Ogawa, and M. Takahashi, "Challenge of ultra high frequency limit of permeability for magnetic nanoparticle assembly with organic polymer—Application of superparamagnetism," *J. Magn. Magn. Mater.*, vol. 321, no. 7, pp. 746–749, Apr. 2009, doi: 10.1016/j.jmmm.2008.11.041.

[98] G. Barrera, P. Allia, and P. Tiberto, "Magnetization dynamics of superparamagnetic nanoparticles for magnetic particle spectroscopy and imaging," *Phys. Rev. Appl.*, vol. 18, no. 2, Aug. 2022, Art. no. 024077, doi: 10.1103/physrevapplied.18.024077.

[99] K. O'Grady and A. Bradbury, "Particle size analysis in ferrofluids," *J. Magn. Magn. Mater.*, vol. 39, nos. 1–2, pp. 91–94, Nov. 1983, doi: 10.1016/0304-8853(83)90407-9.

[100] R. G. Grainger, "Some useful formulae for particle size distributions and optical properties," Dept. Phys., Univ. Oxford, Oxford, U.K., Tech. Rep., Jul. 2025, pp. 6–18. [Online]. Available: https://eodg.atm.ox.ac.uk/user/grainger

[101] T. T. Taylor, "Magnetic polarizability of a short right circular conducting cylinder," *J. Res. Nat. Bur. Standards Sect. B Math. Math. Phys.*, vol. 64, no. 4, pp. 199–210, Oct./Dec. 1960, doi: 10.6028/jres.064b.021.

[102] J. H. Van Vleck, *The Theory of Electric and Magnetic Susceptibilities*. London, U.K.: Oxford University Press, 1931, pp. 27–32. [Online]. Available: https://archive.org/details/theoryofelectric031070mbp

[103] C. Kittel, *Introduction to Solid State Physics*, 4th ed. New York, NY, USA: John Wiley, 1971, pp. 464–466.

[104] F. Gutiérrez-Mejía and J. C. Ruiz-Suárez, "AC magnetic susceptibility at medium frequencies suggests a paramagnetic behavior of pure water," *J. Magn. Magn. Mater.*, vol. 324, no. 6, pp. 1129–1132, Mar. 2012, doi: 10.1016/j.jmmm.2011.10.035.

[105] A. N. Payne. (Jul. 2021). *The Effect of Dielectric Inside an Inductance Coil*. [Online]. Available: https://www.researchgate.net/publication/353574769

[106] C. G. Malmberg and A. A. Maryott, "Dielectric constant of water from 0° to 100° C," *J. Res. Nat. Bur. Standards*, vol. 56, no. 1, pp. 1–8, Jan. 1956, doi: 10.6028/jres.056.001.

[107] Keysight Technologies, *Solutions for Measuring Permittivity and Permeability With LCR Meters and Impedance Analyzers*, 2024, p. 28. [Online]. Available: https://www.keysight.com/us/en/assets/7018-06683/application-notes/5980-2862.pdf

[108] S. Evans, "Dielectric properties of ice and snow—A review," *J. Glaciol.*, vol. 5, no. 42, pp. 773–792, Jan. 1965, doi: 10.3189/s0022143000018840.

RONALD B. GOLDFARB (Life Fellow, IEEE) received the B.A. degree in electrical engineering and the M.S. degree in materials science from Rice University, Houston, TX, USA, in 1973 and 1975, respectively; the Ph.D. degree in physics from Colorado State University, Fort Collins, CO, USA, in 1979; and the M.B.A. degree in business administration from the University of Colorado, Boulder, CO, USA, in 1991. He has been working on superconductors, magnetic materials, and magnetic metrology at the National Bureau of Standards and the National Institute of Standards and Technology (NIST), Boulder, since December 1979, initially as a National Research Council Postdoctoral Associate. He was the leader of the NIST Magnetics Group (2000–2015) and was the Chief Editor of the *Journal of Research of the National Institute of Standards and Technology* (2015–2021). He received the IEEE Magnetics Society Distinguished Service Award in 2016, the IEEE Council on Superconductivity Max Swerdlow Award in 2021, and was inducted into the IEEE Eta Kappa Nu Honor Society in 2018. He served as the Editor-in-Chief of IEEE TRANSACTIONS ON MAGNETICS (1995–2004), was the founder and the Chief Editor of IEEE MAGNETICS LETTERS (2010–2019), and led the establishment of IEEE TRANSACTIONS ON QUANTUM ENGINEERING (2019–2020). He is currently the President of the IEEE Magnetics Society (2025–2026).